Data supplement for Lutz et al., Association of a History of Child Abuse With Impaired Myelination in the Anterior Cingulate Cortex: Convergent Epigenetic, Transcriptional, and Morphological Evidence. Am J Psychiatry (doi: 10.1176/appi.ajp.2017.16111286)

SUPPLEMENTARY MATERIAL

Contents

Supplementary Material and Methods

Human samples

Postmortem Anterior Cingulate Cortex (corresponding to BA24 and BA32) brain tissue was obtained in collaboration with the Quebec Coroner's Office and the Suicide section of the Douglas-Bell Canada Brain Bank (http://www.douglas.qc.ca/page/brain-bank, Montreal, Canada). This study included (i) subjects who died suddenly without prolonged agonal state or protracted medical illness, and with no history of suicidal behavior or psychiatric disorder (Controls), (ii) subjects who died by suicide in the context of a major depressive episode, and who have a history of severe child abuse (Child Abuse) and (iii) subjects who died by suicide in the context of a major depressive episode, but without any history of child abuse (Depressed). Sample characteristics are presented in **Table S1**. Controls, Child Abuse and Depressed groups were matched for age, post-mortem interval (PMI) and brain pH. Psychological autopsies were performed by trained clinicians on both controls and cases, with the informants best-acquainted with the deceased, as described previously(1) and as validated by our group and others(2-7). Diagnoses were assigned based on DSM IV criteria. Characterization of early-life histories was based on adapted Childhood Experience of Care and Abuse (CECA) interviews assessing experiences of sexual and physical abuse, as well as neglect(8, 9), and for which scores from siblings are highly concordant(2, 9). We considered as severe early-life adversity reports of non-random major physical and/or sexual abuse during childhood (up to 15 years). Only cases with the maximum severity ratings of 1 and 2 were included. This information was then complemented with medical charts and coroner records. Ethical approval was obtained from The Institutional Review

Board of the Douglas Mental Health University Institute, and written informed consent was obtained from the family before inclusion in the study.

Tissue dissections. Dissections were performed on 0.5 cm-thick coronal sections with the guidance of a human brain atlas (10), see also http://www.thehumanbrain.info/brain/bn_brain_atlas/brain.html). Anterior cingulate cortex samples were dissected in sections equivalent to plate 6 (-30mm from the center of the anterior commissure) of the atlas. Grey matter was taken immediately rostral to corpus callosum genu. The rostral landmark limit was the cingulate sulcus and the caudal landmark limit was the callosal sulcus. White matter of the Anterior Cingulate Cortex was dissected immediately adjacent to the cingulate gyrus grey matter. The lateral landmark limit was corpus callosum radiation.

Relationship to previous studies

Our previous genome-wide study on epigenetic consequences of child abuse was conducted using MeDIP-chip and a promoter array (11). Here, to achieve a base-resolution analysis of DNA methylation, and to uncover potential functional relevance of DNA methylation at both promoters as well as other genomic sites, we took advantage of the RRBS methodology that was recently implemented by our group for use in human *postmortem* brain tissue (12, 13). The sample investigated in this study is larger and only partially overlapping with that used in previous studies.

Reduced Representation Bisulfite Sequencing (RRBS)

Library preparations. RRBS libraries were prepared as previously described(12, 13). Briefly, 5 µg of genomic DNA was used to carry out overnight MspI (20 units/µg DNA,

New England Biolabs) digestion at 37°C. Digested DNA was purified by phenol/ chloroform extraction, precipitated in the presence of NaCl (0.3 M final) and glycogen (25 µg final), pelleted via centrifugation, rinsed with 80% ethanol, centrifuged again (12000 rpm, 20 minutes), and then resuspended in 100 µl dH20. Satellite bands produced by MspI digestion were checked using an Agilent Bioanalyser. Following MspI digestion, the NEB Next DNA Library Prep Master Mix Set for Illumina was used for Filling-in and A-tailing reactions, according to the manufacturer's instructions. We then used the two-step Illumina adaptor design for DNA library amplification and size selection. Prior to adaptor ligation, we carried out an adaptor Y-fork annealing reaction by combining equal molar ratios of methylated PE1 and methylated PE2 adaptors, with the following denaturing and annealing steps on a thermal cycler: 95°C, 120 s; 80°C, 60 s; 70°C, 60 s; 60°C indefinitely. For the ligation of methylated Y-adaptors to dA-tailed DNA fragments, we used 25 µL dA-tailed DNA, 10 µL NEB Quick ligation Reaction Buffer (5X), 10 µL pre-annealed Illumina methylated Y-adaptors, and 5 µL NEB Quick T4 ligase, incubated for: 16°C, 1 hour; then 20°C, 30 minutes. Adaptor-ligated libraries were purified using the QiaQuick PCR purification kit, and bisulfate-converted using the Qiagen EpiTect Fast 96 Bisulfite Kit. Bisulfate-converted libraries were amplified using the uracil-tolerant Pfu turbo Cx Hotstart DNA polymerase, and size-selected using the progressive PCR method: (1) 95°C-90 s, (2) 95°C-30 s, (3) 60°C-30 s, (4) 72°C-30 s, and (5) 4°C indefinitely - Repeat steps 2–4 for 26 cycles. Samples showing faint but visible 150–400 base pair (bp) smearing on a gel electrophoresis have the optimal amplification PCR cycles. Libraries were then purified using Agencourt AMPure XP beads using a 60 µl/55 µl beads/DNA ratio and quality checked using an Agilent

Bioanalyzer 2100 High Sensitivity DNA Chips. Finally, libraries were indexed during 4 additional PCR cycles, purified, and quantified (see (12) for more details). Five libraries were run per lane of an Illumina HiSeq 2000 flow cell (50bp single-end), at the Génome Québec Center, Montreal, Canada (≈22 million reads/library, **Table S2**). Libraries from Controls and Child Abuse subjects were randomized across sequencing lanes.

RRBS differential methylation calling. We used Trim Galore for quality and adaptor trimming, and Bismark (14) (and Bowtie2) to map sequencing reads to the human reference genome hg19 (allowing two mismatches), and to evaluate bisulfite conversion rates (**Figure S1C**). The DNA methylation percentage was calculated for each cytosine in a CpG context as the unconverted (cytosines) read counts divided by total read counts (cytosines and thymines). In preparation for differential methylation analysis and using the Bumphunter clusterMaker function (https://github.com/ririzarr/bumphunter) (15), we defined genomic windows as any CpG within 50 bp of another CpG, with no limit on the number of CpGs in a given window, but with a minimum of at least 2 CpGs. The CpGs included in differential methylation analyses were determined as follows: (i) only CpG dinucleotides with >5X coverage were included; (ii) only CpG dinucleotides informed in >15 subjects in each Controls and Child Abuse groups were included, (iii) for each subject contributing to differential methylation analysis in a given genomic window, at least two thirds of the CpG sites in that window were informed, (iv) the 0.1% of CpG dinucleotides showing the highest coverage (which may potentially be biased by PCR amplification) were discarded. For each genomic window a differential methylation analysis was performed between Controls and Child Abuse groups (i) using a GLM with group as fixed factor and age and gender as covariates, (ii) treating CG sites

independently in a given genomic window, and (iii) applying the Benjamini-Hochberg procedure for multiple testing corrections (with 0.1 as the threshold for genome-wide significance).

Fluorescence-Activated Cell sorting of oligodendrocyte and neuronal nuclei

Nuclei preparation. Frozen samples were homogenized in nuclei buffer (10mM PIPES [pH 7.4], 10mM KCl, 2mM MgCl2, 1mM DTT, protease inhibitor cocktail (P8340 from Sigma-Aldrich: 104 mM AEBSF, 80 µM aprotinin, 4 mM bestatin, 1.4 mM E-64, 2 mM leupeptin and 1.5 mM pepstatin A) with 0.1% Triton-X, and layered on a cushion of 0.8M sucrose solution before centrifugation at 2500 x g for 20 minutes at 4°C. Pellets were re-suspended in nuclei buffer, centrifuged another round at 2500 x g for 20 minutes at 4°C, and pellets re-suspended in blocking buffer (1% normal donkey serum, 0.5% bovine serum albumin in PBS) containing primary antibodies against Sox10 (1:100; R&D systems) and NeuN (1:500; Alexa700-conjugated, Novus). After washing, nuclei were incubated for 1 hour with species-specific fluorophore-conjugated secondary antibodies (Alexa Fluor 488, 1:500) for the detection of Sox10+ nuclei and washed. Vybrant® DyeCycle™ Violet Stain was added to the nuclei solution prior to flow cytometry analysis. Negative and isotype controls were performed to ensure staining specificity.

Cell sorting. A first gating was applied to discard aggregated doublets and triplets using physical parameters and Vybrant Violet fluorescence (405 nm laser, 525/50 filter). Three non-overlapping gates were then adjusted to collect neuronal nuclei based on NeuN-Alexa700 immunoreactivity (640 nm laser, 730/45 filter), oligodendrocyte nuclei

based on Sox10-Alexa488 immunoreactivity (488 nm laser, 530/30 filter) and the negative fraction. Fractions were collected in PBS and stored at -20°C until DNA extraction. Technical purity of sorted fractions was ensured by sorting the fractions again in a post-sort analysis. Flow cytometry analyses and sorting were performed on a FACSAria Fusion (BD Biosciences) cytometer.

Targeted bisulfate-sequencing (RRBS validation on FACS-sorted nuclei)

DNA extractions. 20 µL of proteinase K was added for every 200K FACS-sorted nuclei, followed by overnight incubation at 56°C in a rotating oven. The samples were then mixed with 770 µL of 20% PEG-8000 2.5M NaCl and 200 µL of AMPure XP Beads for every 200K nuclei, and incubated for one hour at room temperature. DNA extraction was subsequently conducted according to Agencourt's recommendations using a DynaMag™-5 Magnetic stand. DNA concentration was measured using the the Quant-iT™ PicoGreen® dsDNA Assay Kit (ThermoFischer Scientific).

Libraries preparations. We used a PCR-based library preparation procedure (16). Briefly, genomic DNA was bisulfite converted as described above. A first round of PCR amplification was performed on bisulfite-converted DNA (BS-DNA) using the Kapa HIFI Uracil+ mastermix. Primers (**Table S3**) were designed using the MethylPrimer Express software v1.0 (ThermoFischer Scientific). BS-DNA was PCR amplified on a ProFlex thermocycler: 95°C, 3 minutes; then 45 cycles of 98°C for 20s, 58 to 62°c (depending on the primer pair used) for 15s, 72°C for 15s, and finished with 72°C for 1min. Next, PCR amplicons were purified using AMPure Beads at a 1x concentration. A second round of PCR (10 cycles) was then performed using "universal" primers (see **Table S4**)

and the same conditions described above. The PCR reaction was again purified with AMPURE, and a third round of PCR (10 cycles) was performed to add Illumina adapters (P5 and P7) and indices (see primers in **Table S5**). After a final purification, libraires were quantified using an Agilent TapeStation. All samples were normalized based on their molarity, pooled, denaturated using NaOH, diluted to a final 8 pM concentration, and loaded onto an Illumina MiSeq. Libraries were sequenced with the v3, 600-cycle kit to perform 300bp paired-end sequencing, using custom sequencing primers (see(16)).

Bioinformatic analyses. Universal primers sequences were trimmed and sequencing reads with a Phred quality score less than 20 were discarded. The remaining reads were aligned to the human genome hg19, as previously described(12, 17). CpG dinucleotides with a lower than 10x coverage were removed. The DNA methylation percentage was calculated for each cytosine in a CpG context as the unconverted (cytosines) read counts divided by total read counts (cytosines and thymines). Statistical analyses were performed using repeated 2-way ANOVAs with CG sites and groups as main variables, using Prism (GraphPad Software). In case of significant interaction, post-hoc comparison at the level of individual CG sites were conducted using Tukey's.

RNA-Sequencing

RNA was extracted from homogenized brain samples using the RNeasy Lipid Tissue Mini Kit (Qiagen). Quantity and quality of extracted RNAs were measured using an Agilent 2100 Bioanalyzer, and only samples with a RNA integrity number (RIN) greater than 5 were used (N=24 and 26 subjects in the Controls and Child Abuse groups, respectively). RNA-Sequencing libraries were prepared by expert technicians at the

McGill University and Genome Quebec Innovation Center, using the TrueSeq Stranded Total RNA Sample Preparation kit (Illumina), using the Ribo-Zero Gold kit (Illumina) for depletion of ribosomal RNA, followed by first and second strand cDNA synthesis and fragmentation of dsDNA. Then, fragmented DNA was used for A-tailing, adaptor ligation and 12 cycles of PCR amplification. Libraries were quantified using high sensitivity chip on a Labchip (PerkinElmer), quantitative PCR (KAPA Library Quantification, Kapa Biosystems), and PicoGreen (Life Technologies). Three libraries were run per lane of an Illumina HiSeq 2000 (100bp paired-end), yielding ≈62 million reads/library (**Table S6**).

Differential expression analysis. As described previously (17), we used : FASTX-Toolkit (http://hannonlab.cshl.edu/fastx_toolkit/links.html) and Trimmomatic (18) for adapter trimming; Bowtie2 for alignment ; TopHat (19) for transcript counting ; and DESeq2 (20) for differential expression analysis, as previously described (21, 22).

Alignment. Following high-throughput sequencing, 100bp paired-end reads were aligned to the hg19 human genome using TopHat v2.1.0 (http://tophat.cbcb.umd.edu/) with a mate insert distance of 75 bp (-r) and library type fr-unstranded. Reads passing a mapping quality of at least 50 were used for gene and transcript quantification.

Quantification. Gene annotations from the Ensembl release 75 were used for quantification. For gene-level quantification we used HTSeq-count version 0.6.1p1 (http://www-huber.embl.de/users/anders/HTSeq/doc/overview.html) (23), using the intersection-nonempty mode, and results were combined to form a count matrix of 20,893 transcribed RNAs across 50 samples. *Differential expression analysis*. Genes with no mapped fragments were removed from the analysis. Furthermore, genes with low counts were removed by keeping only those with at least 10 counts per subject in

average. Differential expression analysis was performed using the DESeq2 GLM using the following covariates: gender (24), age (25), and RIN (26), based on previous literature documenting their impact on human brain RNA-Seq datasets.

Gene Set Enrichment Analysis (GSEA). GSEA was performed as previously described (27). Log_2 fold changes were obtained for each gene from the differential gene expression analysis. Genes were ranked based on their fold changes where genes with the highest positive fold changes were at the top of the list and those with the lowest negative fold changes were at the bottom of the list. The ranked gene list was then used as an input for the GSEAPreranked tool, with the "classic" enrichment score calculation option selected. The C2 curated gene sets molecular signatures database was used to identify enriched gene sets.

RT-PCR analysis of gene expression

RNA was extracted from brain tissue using the RNeasy Lipid Tissue Mini Kit (Qiagen). RNA quantity and quality were measured as described above, and only samples with RIN>5 were used. Extracted RNA was reverse-transcribed using M-MLV reverse transcriptase (Invitrogen™). mRNA levels were quantified by real time polymerase chain reaction (RT-PCR) using SYBR® Green DNA intercalating dye and master mix (Bio-Rad) and the ABI 7900HT PCR machine. Primers for the ITGB1 (**Table S7**) gene were designed using Primer-BLAST (http://www.ncbi.nlm.nih.gov/tools/primer-blast/), and validated by gel migration and dissociation curves. Relative expression levels for the gene of interest were calculated using calibration curves and two reference housekeeping genes (GAPDH and β-actin) (28). A general linear model was used to

analyze group differences as a function of histories of child abuse or depressive psychopathology. The RIN and age covariates, which were found to significantly affect this gene's expression in the RNAseq dataset, were used in the final model.

Nanostring analysis of gene expression (RNA-Sequencing validation)

Experiments were performed at the Jewish General Hospital Molecular Pathology Centre (Montréal, QC, Canada) using Nanostring nCounter targeted gene expression profiling (29), as described previously (30). Briefly, 5 μl of total RNA (20 ng/μl) was hybridized with the reporter and capture probes at 65^{o}C in a thermocycler for 19-20 hours. Probes were designed against 35 myelin-related genes and 5 housekeeping genes as internal controls: ACTB, RPL13, RPLP1, PDE4DIP, ARHGEF12. The samples were then processed with the nCounter Prep Station to purify the hybridized targets and affix them to the cartridge. After transfer to the nCounter Digital Analyzer, barcodes were counted and tabulated for each target molecule. The data were analyzed using the nSolver version 2.6.43 following the manufacturer's recommendations.

Animals and maternal behaviour

Maternal behaviour was scored as previously described (31-33). The frequency of maternal licking and grooming (LG) behaviour was scored on postpartum days 1–6. Observers were trained to a high level of interrater reliability (greater than 0.90). Dams were observed in their home cage and undisturbed for the duration of the observation period. Daily observations occurred during five 75 min sessions: three occurring during the light phase (10.00, 13.00 and 17.00 h) and two during the dark phase (07.00 and

20.00 h) of the light cycle. Within each observation session, the behaviour of each mother was scored 25 times (one observation per 3 min) for pup LG (including both body and anogenital licking). Thus, the frequency score of pup LG was expressed as percentage occurrence (number of occurrences per number of observations x 100%). Mothers were designated as high or low LG dams on the basis of the pup LG frequency score relative to the mean ± 1 standard deviation for the cohort (generally 40–60 mothers per cohort). Accordingly, high LG mothers were defined as females for which the LG frequency scores were greater than 1 standard deviation above the cohort mean. Low LG mothers were defined as females for which the LG frequency scores were greater than 1 standard deviation below the cohort mean.

Immunohistochemistry

After quenching of endogenous peroxidase with H_2O_2 and blocking in 10% normal serum/PBS/Triton-X 0.3%, 50µm thick sections were incubated overnight with primary antibodies (goat anti-PDGFRα, 1:100, R&D Systems AF-307-NA; goat anti-Sox10, 1:500, R&D Systems AF2864), followed by incubation with respective biotinylated secondary antibodies (goat anti-rabbit, 1:500; horse anti-goat, 1:500; Vector Laboratories). The signal was detected by DAB following avidin-biotin complex amplification with Vectastain Elite ABC kit (Vector Laboratories). For PDGFRα staining sections were first incubated in 1:1000 proteinase K (Qiagen) for 10 minutes prior to H_2O_2 treatment.

***Stereology*.** An optical fractionator probe (Stereo Investigator, MBF) was used to obtain unbiased estimates of oligodendrocyte-lineage cells (Sox10+) and oligodendrocyte

precursor cells (PDGFRα+). Systematic random sampling was done with a section sampling fraction of 1/6 on an Olympus BX51 microscope (motorized stage and CX9000 camera, MBF). Based on a pilot study (Gundersen CE (m=1) < 0.07), a sampling grid of 750µm x 750µm was used, with counting frames of 30µm x 30µm or 100µm x 100µm for Sox10 and PDGFRα, respectively. Dissector height was set at 14µm, with 2µm guard zone distance, and cells were counted at 40x magnification (0.75 NA, UPlan FL N objective). Volume of the total area sampled per subject was determined using the Cavalieri Estimator probe (grid spacing of 100µm, 50µm thickness). Cellular densities were calculated by dividing their respective population estimates by the Cavalieri volume estimation.

Coherent Anti-Stokes Raman Scattering (CARS) microscopy

Tissue preparation. For CARS imaging, frozen white matter blocks of adjacent white matter from the anterior cingulate cortex were fixed in 10% formalin overnight at 4°C, rinsed thoroughly in PBS and 300µm thick sections were cut directly on a vibratome (Leica VT1200S) in ice cold PBS. Sections were then stored in cryoprotectant at -20C until CARS imaging.

CARS imaging setup. The polarization resolved CARS setup is based on a custom-build, video-rate, laser scanning microscope and two laser sources (Figure 4A). An 80 MHz, 7 ps mode-locked laser (Nd:YVO4, High-Q Laser, Austria) delivers the Stokes pulse at 1064 nm, and its second harmonic synchronously pumps an optical parametric oscillator (OPO) (Levante Emerald, APE), generating a pump beam which is set at 817 nm to probe CH2 stretching bands in myelin (2845 cm−1). The pump and the Stokes

beams are recombined spatially and temporally using a delay line. The laser beams are focused in the sample using a high-numerical aperture water-immersion objective (60x, 1.2NA, UIS-UPLAPO, Olympus). Images are performed by raster beam scanning a sample (gold-coated polygonal mirror for the fast axis, Lincoln Laser, DT-36-290-025, a galvanometer mirror for the slow axis, Cambridge Technology 6240H) at a rate of 30 images per second (2252x500 pixels, scan range 308x65 µm) and with an average power at the focal spot of 5-15mW. The backscattered anti-Stokes signal (662 nm) is separated from the excitation beam by a dichroic long-pass filter (Semrock, FF735-Di01) and a short-pass filter (Semrock, FF01-750/SP-25) and collected in the epi-direction by a red-sensitive photomultiplier tube (Hamamatsu, R3896). One image is recorded for each direction of the incident linear polarizations, tuned from 0º to 180º (in 3º steps) by rotation of an achromatic half-wave plate mounted on a step motor at the entrance of the microscope. The polarization distortions originating from the last dichroic mirror are compensated by introducing a second identical dichroic in the light path(34).

Segmentation. To extract nerve fiber morphometric information of human brain tissue we applied a segmentation algorithm designed for CARS images(35). First, an image stack recorded for different polarization states is averaged over all incident polarizations to create one image (Figure 4B). Next, the method classifies each pixel and assigns it either to axon or to myelin. The axon segmentation is divided into three steps: 1) groups of pixels corresponding to a local minimum of at least a certain depth (extended-minima algorithm) are identified as axon candidates regardless of their shape, 2) their shape is refined through an iterative deformation process (active contour algorithm) 3) the axon candidates are subjected to a first validation test that aims to identify and remove inter-

nerve-fiber background based on morphological properties. The myelin segmentation strategy comprises three steps: 1) the myelin outer boundary of axon candidates is detected in the straightened subspace image when the intensity changes from high to low, 2) the candidates are subjected to a second validation test based on the area overlap between neighboring nerve fibers, and 3) all unique pairs of touching segmented myelin are pairwise separated using a watershed algorithm. For this project, all fibers identified by the segmentation algorithm were also manually validated. For each selected nerve fiber, standard morphometric measurements were computed from the segmentation results using Matlab (Mathworks): axon and fiber diameter (i.e., axon plus myelin sheath), myelin thickness, g-ratio. Statistical analysis was performed on R and Prism (GraphPad Software). One- and two-way ANOVAs with or without repeated measures were performed for main and interactive effects, followed by Tukey's HSD for post-hoc comparisons.

Polarization-resolved CARS microscopy. The principle of the technique relies on simultaneous tuning of the incident linear polarizations of pump and Stokes beams. Several images of a sample are recorded for linear, regularly spaced input polarization directions in the sample plane, ranging between 0° (along the horizontal axis of the image) and 180° (**Figure S10**). The polarization-resolved CARS intensity can be written as a two-termed harmonic Fourier series:

$$I(\varphi) = a_0 + a_2\cos(2\varphi) + b_2\sin(2\varphi)$$
$$+ a_4\cos(4\varphi) + b_4\sin(4\varphi)$$

where φ is the incident polarization angle with respect to the x axis in the sample plane, and a_n and b_n are the coefficients of the Fourier series representing *nth* order of

symmetry(36). These coefficients can be redistributed to define the magnitude of the *n*th order symmetry component:

$$C_2 = \sqrt{a_2^2 + b_2^2} \quad \text{and} \quad C_4 = \sqrt{a_4^2 + b_4^2}$$

Every polarization stack is thus represented by its symmetry spectrum (C_2, C_4). Finally, molecular organization, called here molecular order, can be defined as a modulation magnitude of the symmetry components resulting from the change of polarization:

$$\text{molecular order} = \sqrt{\frac{C_2^2 + C_4^2}{C_0^2}} \qquad \text{where } C_0 = a_0$$

This equation, even though it ignores the specific symmetries and averages over *nth* symmetry components, already reveals the essential feature of the molecular distribution: molecular order reaches maximum for pure *nth* order symmetry (crystalline media) and decreases when the disorder increases (cell membranes, biological media), reaching 0 for an isotropic distribution. The data processing relies on a Fourier series decomposition of the polarization-resolved signal, recorded in every pixel of the image. From this analysis, the information on the local molecule's averaged order is retrieved and images of molecular order provide direct information on the spatial repartition of molecular organization in the sample (**Figure S10**).

Statistical analyses

Differential methylation analysis of RRBS data was performed using a GLM with age and gender as covariates and applying the Benjamini-Hochberg procedure for multiple testing corrections. One-way and two-way ANOVAs (with CpG site as within-subjects factor and group as between-subjects factor) were used to analyse DNA methylation patterns of Sox10+ and NeuN+ nuclear fractions after FACS, followed by Tukey's HSD

post-hoc test for corrected multiple comparisons. For differential gene expression of RNA-Sequencing data, the DESeq2 R module was used to perform GLMs with age, gender and RIN as covariates, and applying the Benjamini-Hochberg procedure for multiple testing corrections. Differential gene expression from the Nanostring validation experiment was conducted similarly with GLMs using child abuse and psychopathology as fixed factors. Cellular densities of Sox10+ and PDGFRα+ cells were analysed using one-way ANOVAs with group as between-subjects factor, followed by Tukey's HSD post-hoc test for corrected multiple comparisons. For myelin morphometry analyses, all variables were analysed using one-way or two-way ANOVAs (with axon caliber category as within-subject and group as between-subject factors), followed by Tukey's HSD post-hoc test for corrected multiple comparisons. Data distribution and homogeneity of variance were assessed using Shapiro-Wilk and Levene's tests respectively, and no data transformation was applied. Significance threshold was set to 0.05. All statistical analyses were performed with R, SPSS (IBM), and Statistica (StatSoft), and represented using Prism (GraphPad).

Supplementary Figures and Tables

FIGURE S1. Reduced Representation Bisulfate Sequencing (RRBS) quality controls.

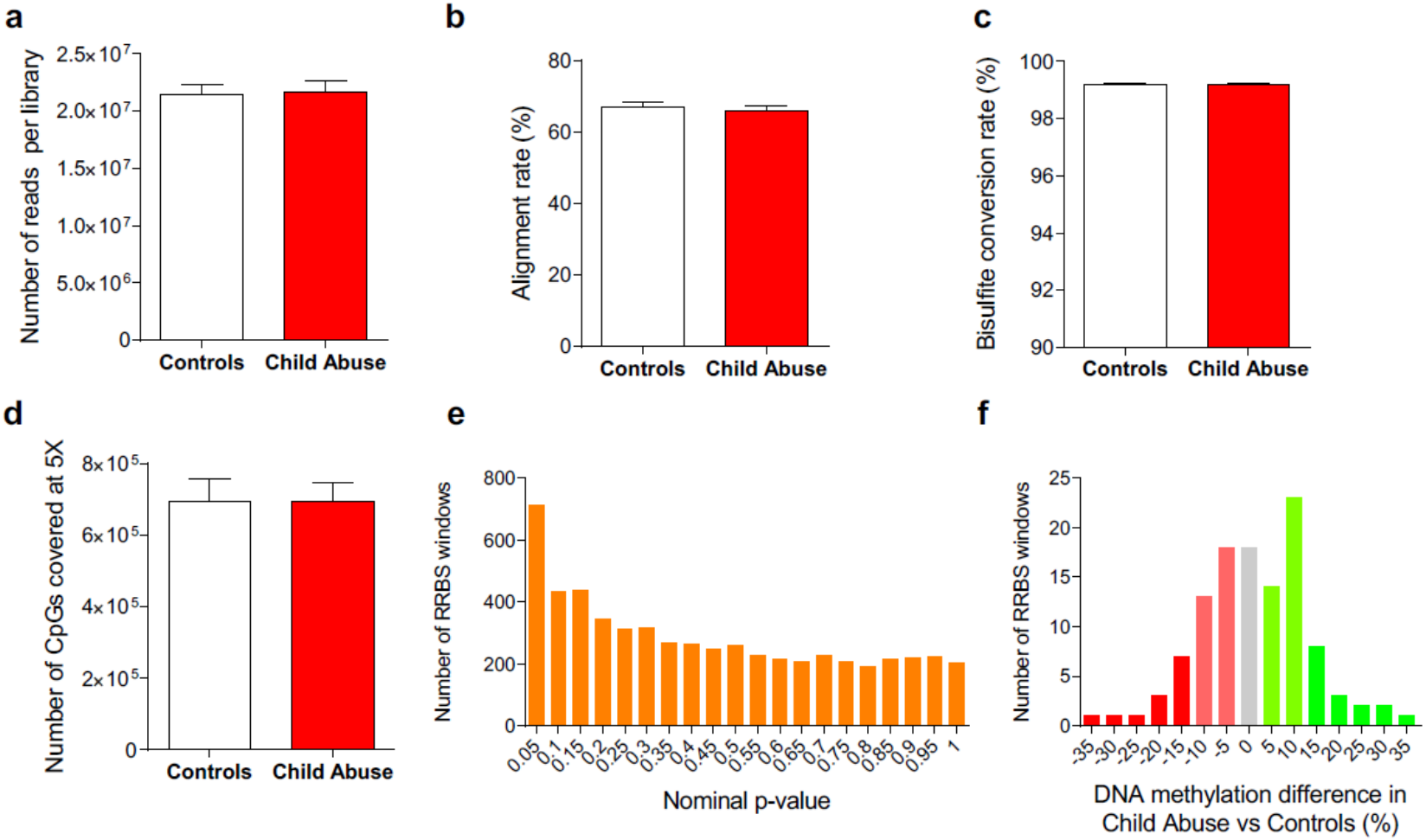

(a) DNA was extracted from anterior cingulate cortex tissue and used to prepare RRBS libraries that were sequenced on the HiSeq 2000 platform (50bp single-end reads), generating similar sequencing depth among Controls and Child Abuse groups. Linear regression analysis found no significant relationship between the number of reads generated and either gender (r^2=0.0003, p>0.05), postmortem interval (PMI, r^2=0.0008,

p>0.05), brain pH (r^2=0.006, p>0.05) or age (r^2=0.06, p>0.05), and there was no significant difference in average read numbers between groups (t-test, p=0.82). (**b**) During alignment to the human reference genome hg19 using Bismark (see Material and Methods), there was no group difference in alignment rates between the Controls and Child Abuse groups (t-test, p=0.63) as well as no correlation with clinical covariates: gender (r^2=0.02, p>0.05), postmortem interval (PMI, r^2=0.008, p>0.05), brain pH (r^2=0.07, p>0.05), age (r^2=0.05, p>0.05). (**c**) Similarly, the bisulfite conversion rate computed by Bismark was very high (99.2±0.02% in all 52 libraries) and similar across both groups (t-test, p=0.90), with no effects of covariates: gender (r^2=0.04, p>0.05), postmortem interval (PMI, r^2=0.04, p>0.05), brain pH (r^2=0.05, p>0.05), age (r^2=8E-5, p>0.05). (**d**) A similar 5X coverage at CpG dinucleotides was achieved in both groups (t-test, p=0.99), with no effect of covariates: gender (r^2=4E-5, p>0.05), postmortem interval (PMI, r^2=0.02, p>0.05), brain pH (r^2=0.007, p>0.05), age (r^2=0.07, p>0.05). (**e**) Distribution of p-values among the 5724 genomic windows that were analysed for differential methylation. (**f**) Distribution of % DNA methylation changes in Child Abuse (N=27) compared to Controls (N=25) subjects among the 115 genomic windows that showed genome-wide significance (q-value<0.1 after Benjamini-Hochberg correction).

FIGURE S2. Total number of nuclei isolated by Fluorescent Assisted Cell Sorting (FACS) from the anterior cingulate cortex

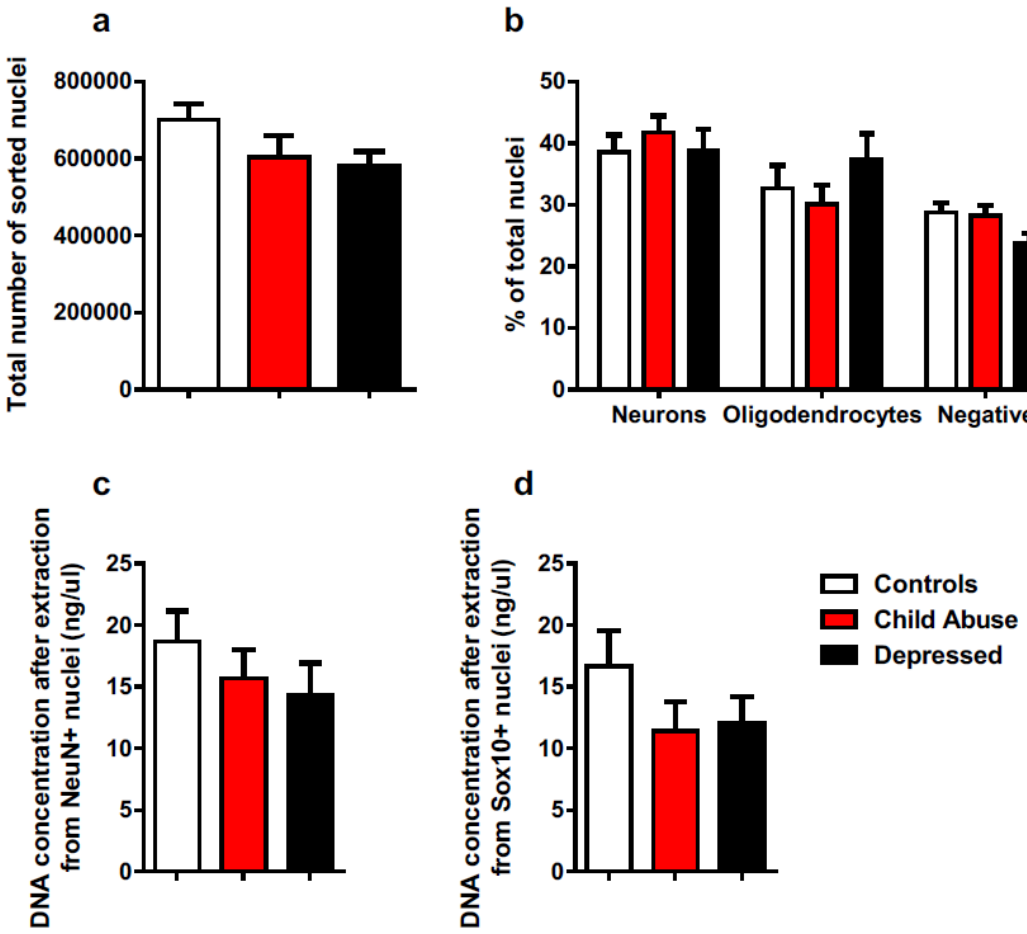

(**a**) The total number of nuclei isolated by Fluorescent Assisted Cell Sorting (FACS) from the Anterior Cingulate Cortex of Controls (N=24), Child Abuse (N=25) and Depressed (N=23) did not differ between groups (one-way ANOVA: $F(2, 72) = 1.883$, $P>0.05$). (**b**) The percentage of neuronal (NeuN+), oligodendrocyte (Sox10+) and negative (NeuN-/Sox10-) nuclei sorted from the Anterior Cingulate Cortex did not differ between groups (two-way repeated measures ANOVA, group effect: $F(2, 75) = 0.8634$, $P>0.05$; cell-type effect: $F(2, 150) = 9.739$, $P<0.05$; group x cell-type interaction: $F(4, 150) = 0.9840$, $P>0.05$). (**c-d**) Mean concentration of DNA extracted from sorted neuronal (**c**) and oligodendrocyte (**d**) nuclei. No difference between groups was observed (NeuN+, one-way ANOVA: $F(2, 71) = 0.8017$, $P>0.05$; Sox10+, one-way ANOVA: $F(2, 72) = 1.345$, $P>0.05$). Data represent mean ± sem.

FIGURE S3.

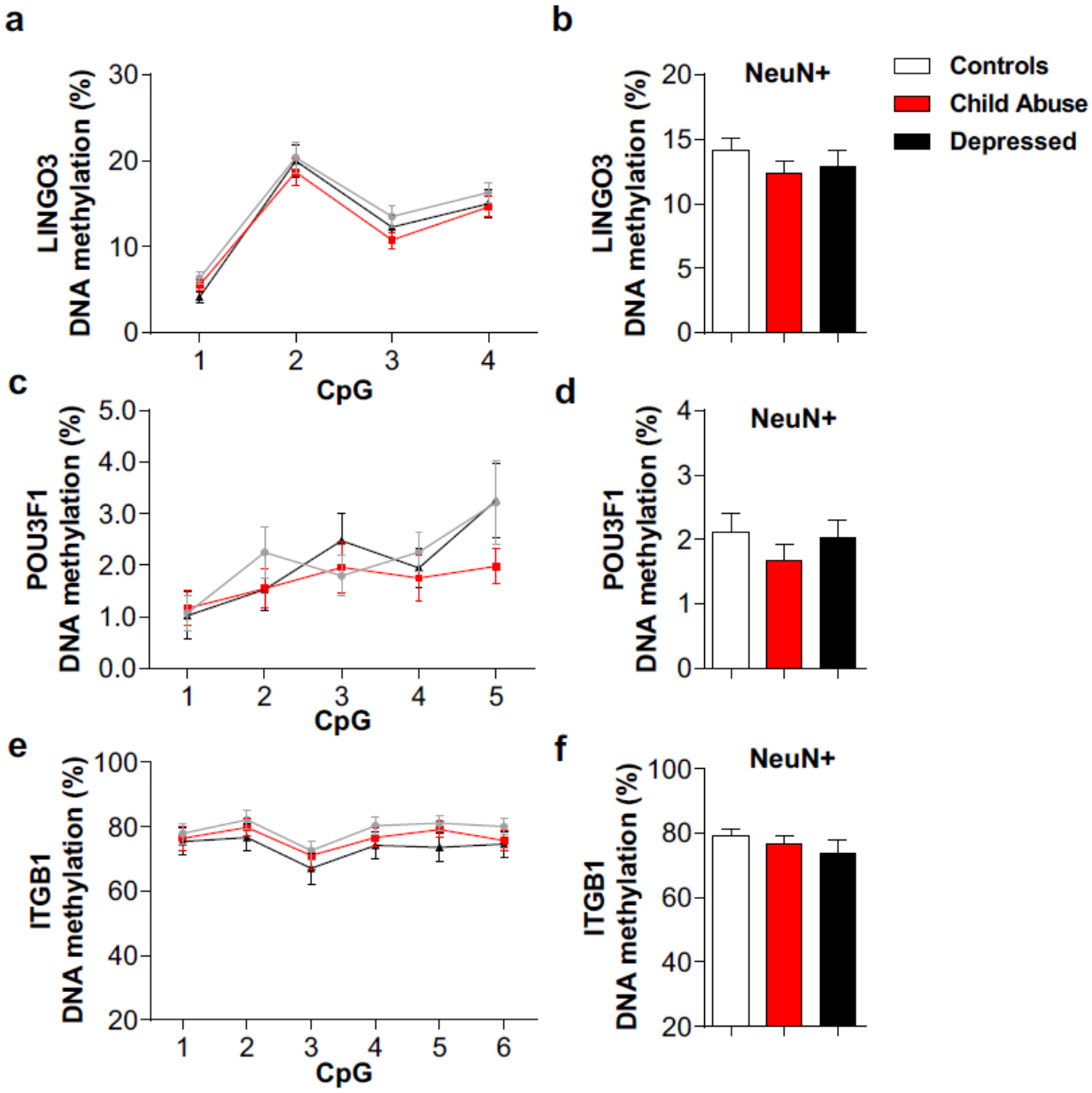

No effects of child abuse nor psychopathology on the patterns of DNA methylation of myelin genes in neuronal (NeuN+) nuclei. DNA methylation patterns of genomic regions previously targeted in oligodendrocyte nuclei (see Figure1) were assessed by targeted-bisulfite sequencing in neuronal nuclei isolated from the Anterior Cingulate Cortex of Controls (N=19-23), Child Abuse (N=25-26) and Depressed (N=20-25). (**a**) LINGO3, two-way repeated measures ANOVA: Group effect: [$F(2, 70)=0.89$, $p>0.05$]; CpG site effect: [$F(3, 210)=75.7$, $p<0.001$]; group x CpG interaction: [$F(6, 210)=0.78$, $p>0.05$]. (**b**) POU3F1, two-way repeated measures ANOVA: Group effect: [$F(2, 69)=0.79$, $p>0.05$]; CpG site effect: [$F(4, 276)=5.96$, $p<0.05$]; group x CpG interaction: [$F(8, 276)=0.80$, $p>0.05$]. (**c**) ITGB1, two-way repeated measures ANOVA: Group effect: $F(2, 62) = 0.6316$, $p>0.05$; CpG site effect: $F(5, 310) = 12.07$, $P<0.001$; group x CpG interaction: $F(10, 310) = 0.4750$, $P>0.05$. Data represent mean ± sem.

FIGURE S4. RNA-Sequencing quality controls

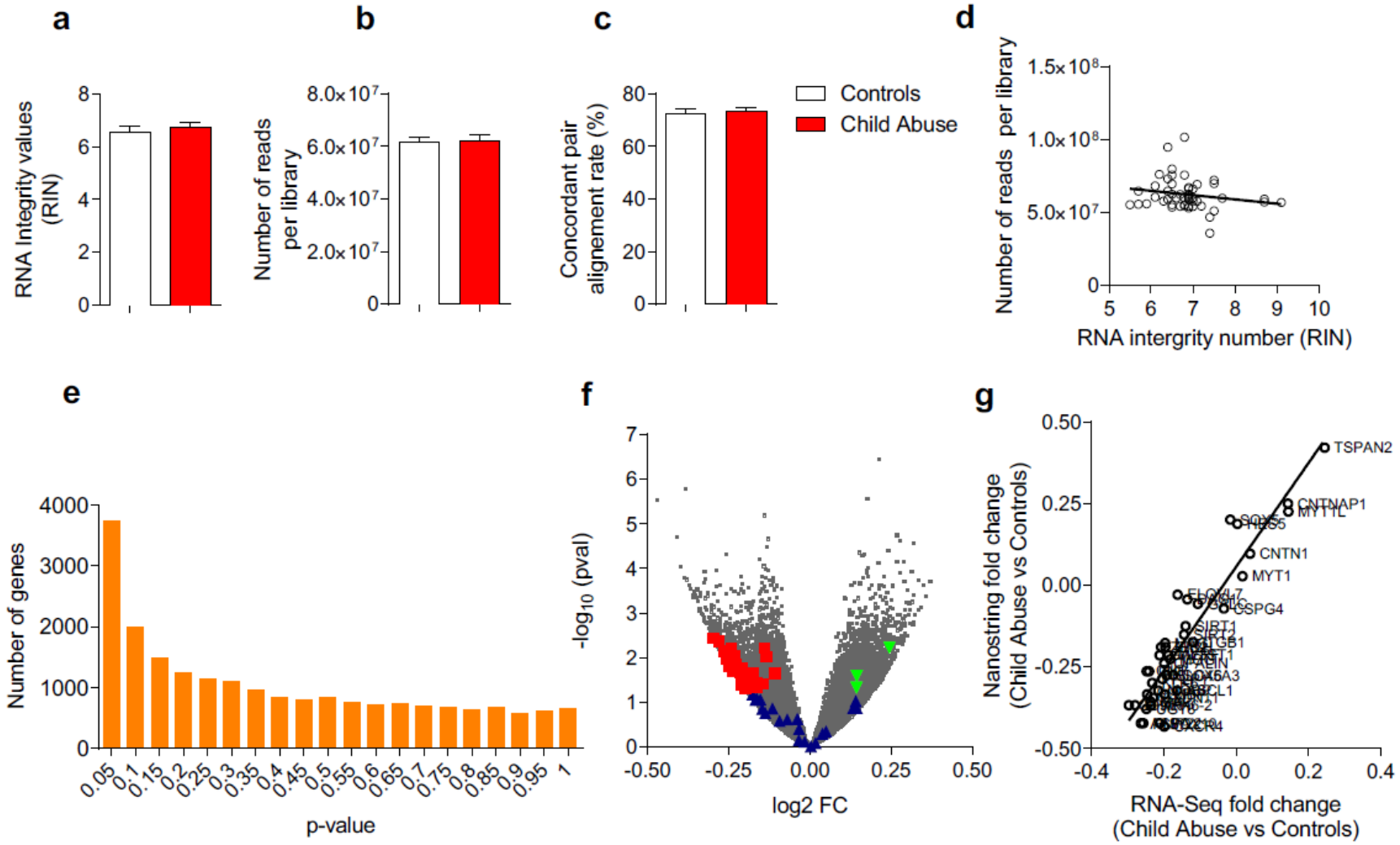

(a) RNA was extracted from anterior cingulate cortex tissue and RNA integrity numbers (RIN) were measured using a BioAnalyzer. Only RNA samples with RIN above 5 were used for RNA-Sequencing library preparation. There was no group difference in RIN values between Controls (N=24) and Child Abuse (N=26) subjects (t-test, p=0.86). **(b)** RNA-Sequencing libraries were sequenced on the HiSeq 2000 platform (100bp paired-end reads) to generate similar sequencing depth among Controls and Child Abuse groups (t-test, p=0.10), with 66.8 ± 0.3 million reads in average across both groups. **(c)** The alignment rate of paired reads was similar across Controls and Child Abuse groups (t-test, p=0.68). (**d**) No

significant correlation was found between RNA integrity numbers (RIN) and the number of sequencing reads. **(e)** Distribution of nominal p-values among the 20893 genes analysed for differential expression between Child Abuse and Control subjects using the DESeq2 generalized linear model (see material and methods). (**f**) Volcano plot showing the bidirectional distribution of the 3734 (17.9% of all genes) genes differentially expressed between Child Abuse (N=24) and Control subjects (N=26): red squares depict the 32 genes that showed a nominally significant downregulation ($p<0.05$); green triangles depict the 3 genes that showed a nominally significant upregulation ($p<0.05$); blue triangles indicate the 20 genes that showed no evidence for differential expression ($p>0.05$). (**g**) Nanostring nCounter targeted gene expression profiling was used to validate RNA-Sequencing results. A strongly significant correlation was found between RNA-Sequencing and Nanostring fold changes [Pearson linear regression, $r^2=0.87$, $p<0.0001$].

FIGURE S5. Permutation testing for the myelin gene collection

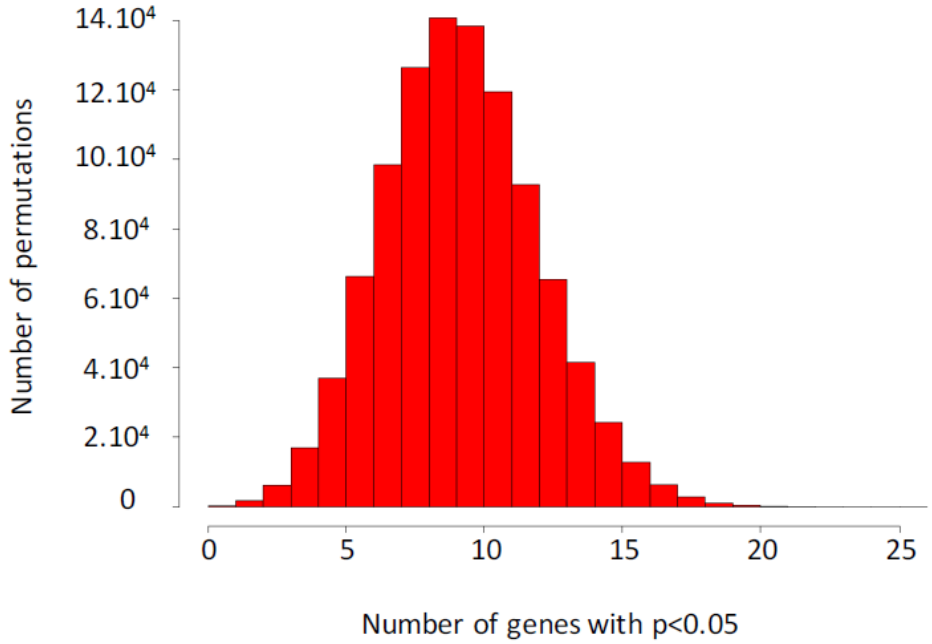

One million lists of 55 genes each were randomly generated using results from the RNA-Sequencing DESeq2 differential expression analysis. For each list, the number of genes showing a nominal p-value below 0.05 was counted. The graph shows the number of lists (y-axis) as a function of the number of nominally significant genes in each list (x-axis). There was no list that matched the number of dysregulated genes observed for our collection of myelin-related genes (N=35), indicating that the observed enrichment is unlikely due to chance.

FIGURE S6. RNA-Sequencing results were validated using Nanostring nCounter targeted gene expression profiling

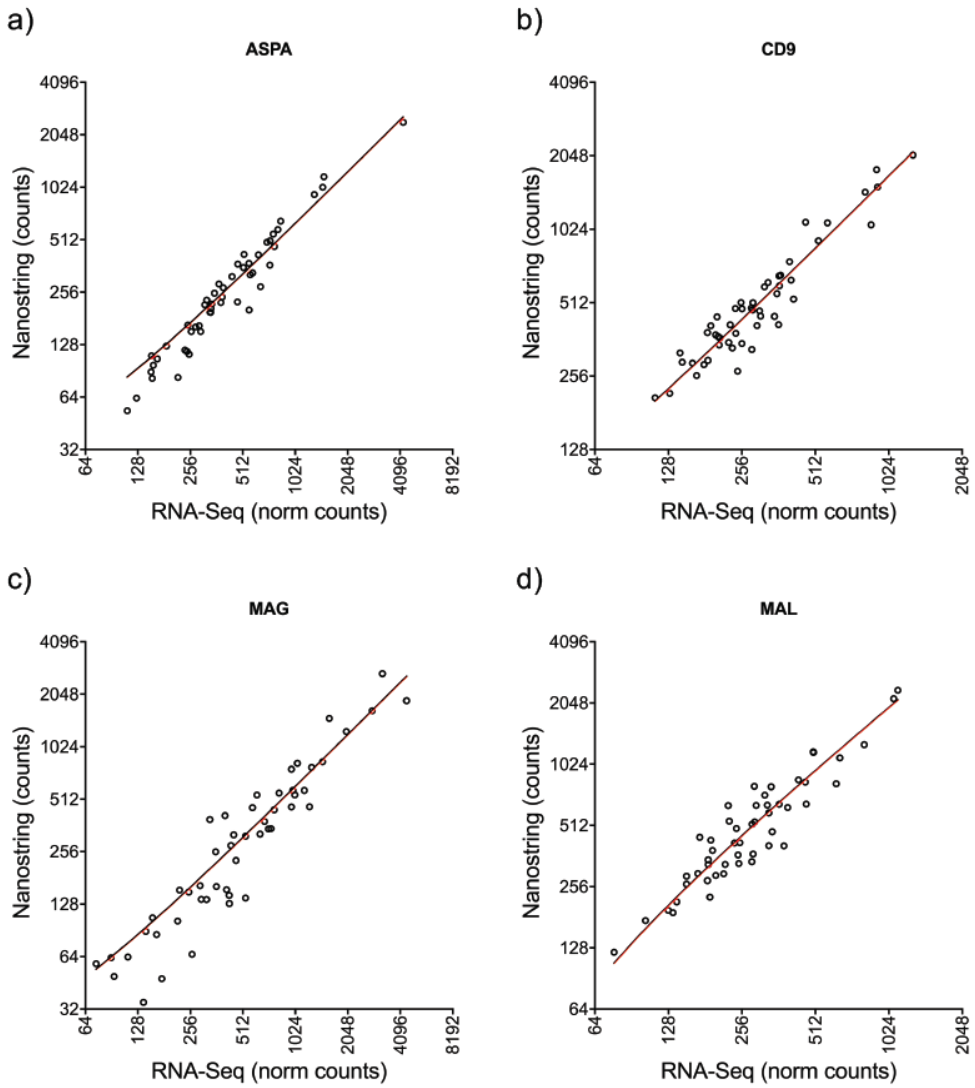

Here, examples of correlations between RNA-Seq and Nanostring results are shown for individual genes. Among others, significant correlations were observed for ASPA: r^2=0.96, p<0.0001 **(a)**; CD9: r^2=0.93, p<0.0001 **(b)**; MAG r^2=0.86, p<0.0001 **(c)**; and MAL r^2=0.90, p<0.0001 **(d)**.

FIGURE S7. RNA-Sequencing results for the β- and α-subunits of integrin proteins

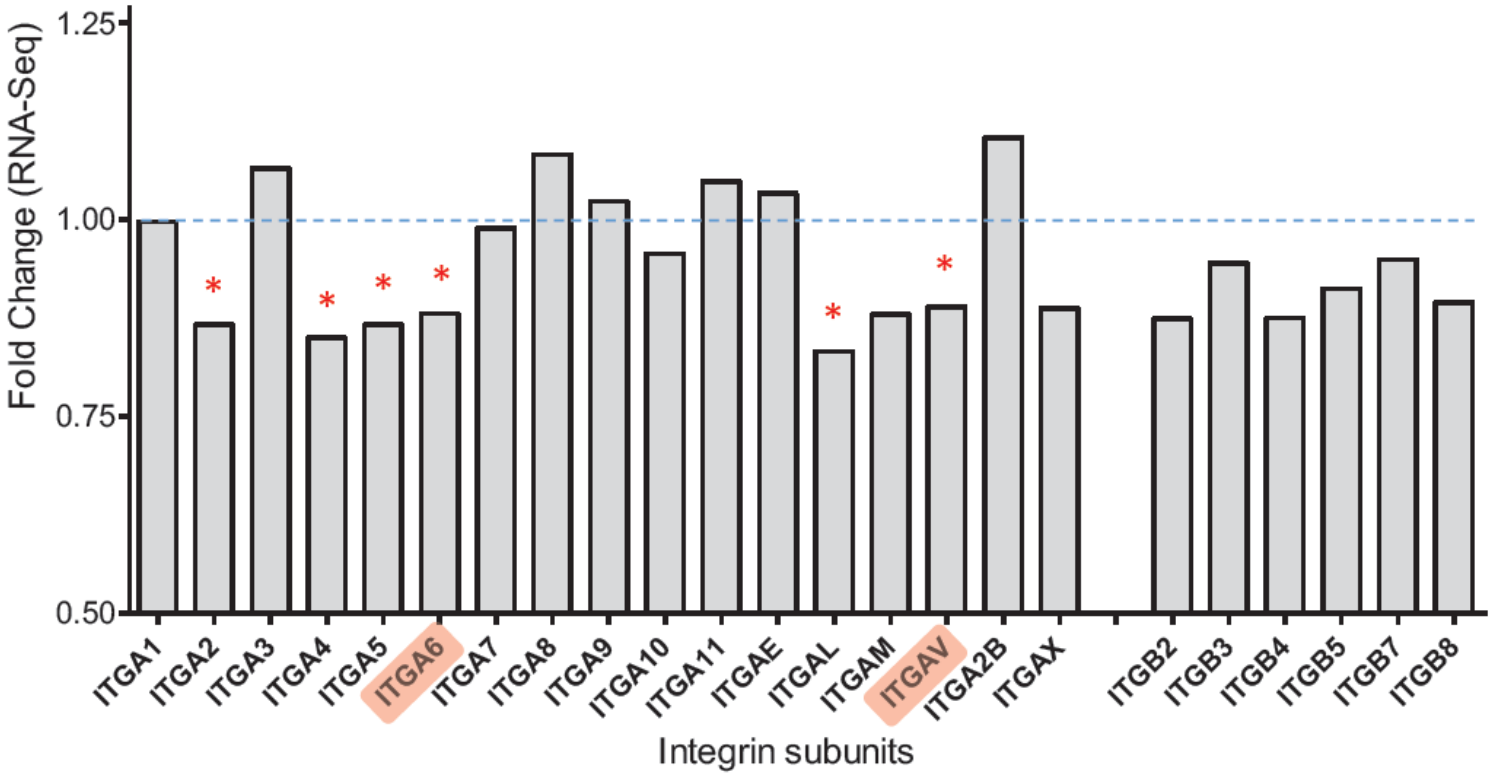

Integrins are transmembrane proteins that form heterodimers. *In vitro* and *in vivo* studies have shown that in oligodendrocytes, the β-subunit ITGB1 forms heterodimers with two main α-subunits, ITGA6 and ITGAV (red squares). As shown here, both α-subunits are nominally downregulated in RNA-Sequencing data comparing Child Abuse subjects and Controls: (i) ITGA6, p=0.015, fold change (FC)=0.88; (ii) ITGAV, p=0.039, FC=0.89. Therefore, integrin signaling is likely impaired in Child Abuse subjects, which may contribute to observed deficits in myelination. Note that four other α-subunits were also down-regulated in Child Abuse subjects, suggesting that other cell-cell interactions might be disrupted in these subjects: (i) ITGA2, p=0.033, FC=0.87 (ii) ITGA4, p=0.016, FC=0.85 (iii) ITGA5, p=0.040, FC=0.87 (iv) ITGAL, p=0.009, FC=0.83. *, p<0.05 in RNA-Sequencing GLM.

FIGURE S8. RNA-Sequencing results for the myelin collection of 55 genes in the anterior cingulate cortex and the lateral amygdala

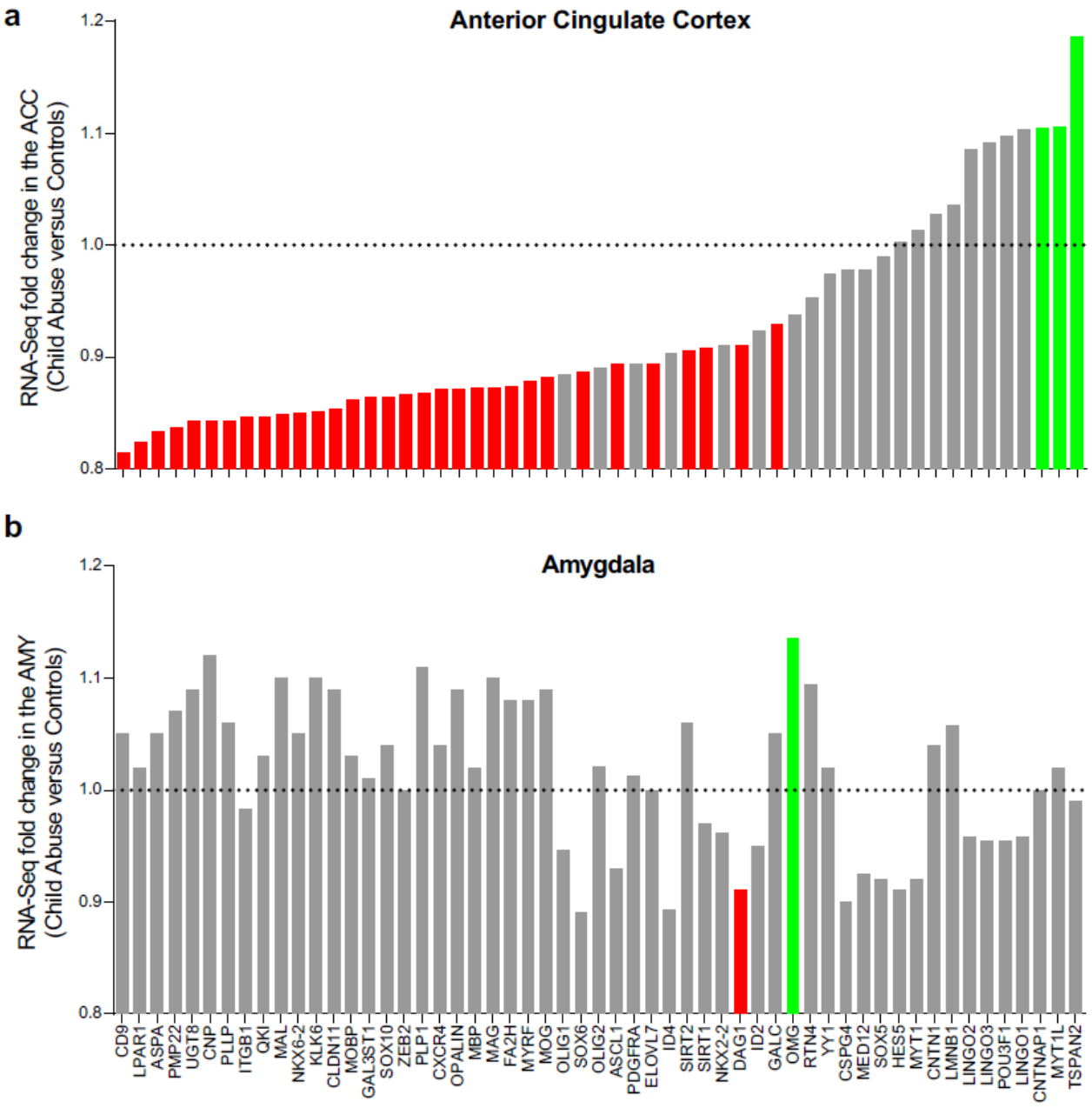

RNA-Sequencing results for the myelin collection of 55 genes in the anterior cingulate cortex (ACC, **a**) and in the lateral amygdala (AMY, **b**). RNA was extracted from the AMY in groups of Controls (N=17) and Child Abuse (N=22) subjects that were all present in the cohort previously investigated in the ACC. RNA-Sequencing libraries were prepared using the same methodology, sequenced at similar depth, and processed for data analysis through the same bioinformatic pipeline across both brain regions. The pattern of myelin-related genes dysregulation that was observed in the ACC **(a)** is virtually absent in the AMY **(b)**, suggesting that child abuse-induced dysregulation of adult myelination might exhibit brain-region specificity. Red bars indicate genes showing nominally significant ($p<0.05$) downregulation in Child Abuse versus Control subjects (RNA-Sequencing GLM), green bars indicate nominally significant ($p<0.05$) upregulated genes, and grey bars indicate genes that are not dysregulated ($p>0.05$).

FIGURE S9. Effects on anterior cingulate cortex myelin gene expression of maternal care in rats and child abuse in humans

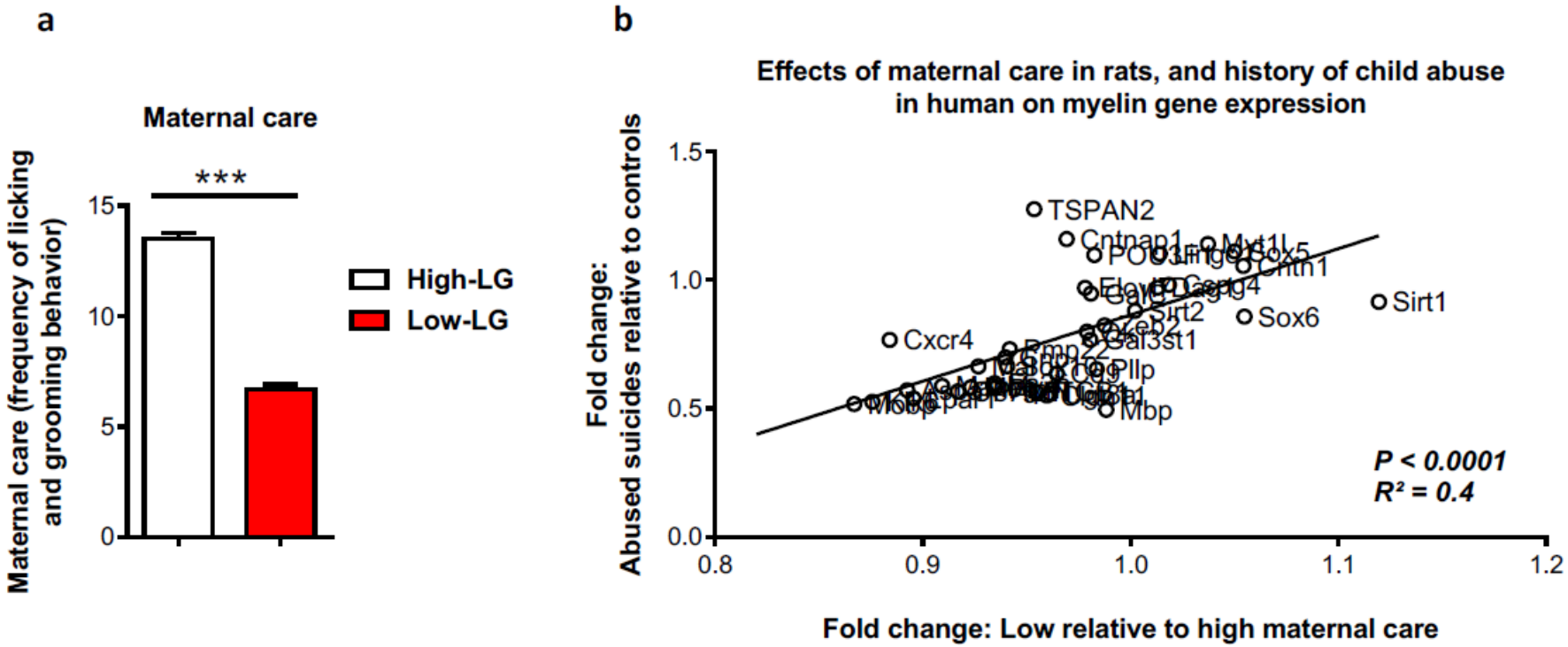

(a) Offsprings raised by dams showing either low (low-LG) or high (high-LG) levels of maternal behaviour were selected to investigate the effects of maternal care variations on myelin gene expression (low-LG versus high-LG: $p<0.001$ by unpaired t-test; data represent mean ± sem, n=12 per group). (**b**) Their myelin genes expression was assessed by Nanostring using rat-specific probes targeting the collection of genes previously interrogated in postmortem human samples from controls and depressed suicides with or without a history of child abuse (see **Fig.2g**). Adult rats raised by low LG dams showed myelin expression changes that were strongly correlated ($p<0.0001$) with myelin genes expression changes observed in humans who experienced child abuse.

FIGURE S10. Child abuse is associated with higher myelin molecular order in fibers of the anterior cingulate cortex

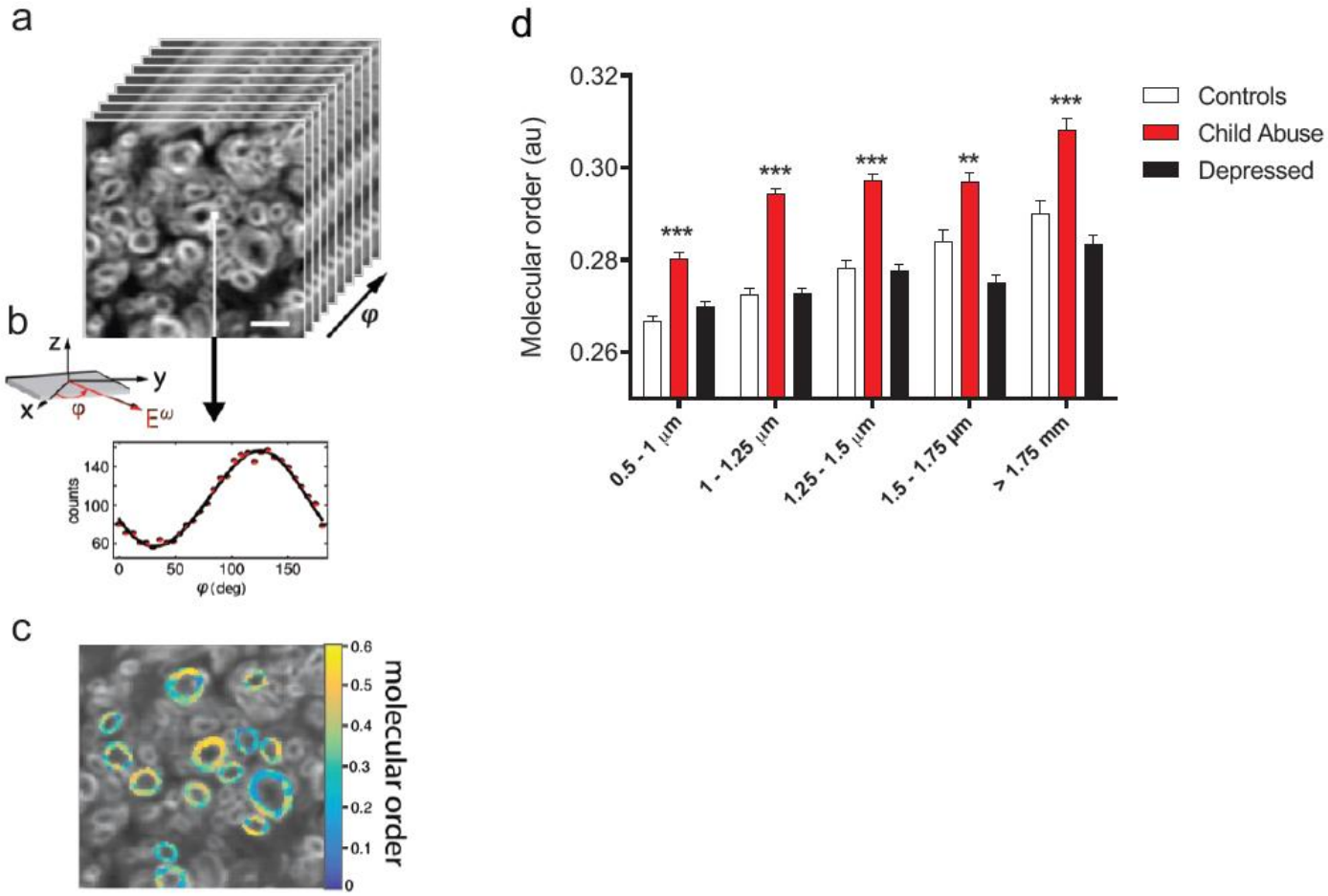

Polarization resolved CARS was used to analyse the molecular order of myelin of individual anterior cingulate cortex fibers (see Material and Methods) of Controls (N= 5597), Child Abuse (N=6090) and Depressed (N=7262) subjects **(a)** Stack of polarization-resolved CARS data from a section of human anterior cingulate cortex. **(b)** Polarization-resolved data recorded for one pixel in an arbitrary chosen fiber are shown with 31 input polarizations (shown schematically in the inset). **(c)** Retrieved image of the local molecular order superimposed with the CARS intensity image in greyscale. **(d)** Child abuse is associated with higher molecular order of myelin for all diameter classes of fibers analysed (Two-way ANOVA, group effect: $F(2, 18934) = 188.0$, $P<0.0001$; class effect: $F(4, 18934) = 62.26$, $P<0.001$; class x group interaction: $F(8, 18934) = 3.903$, $P=0.0001$; for all classes: C versus SA, ***$p<0.001$ by Tukey's HSD; C versus DS, $p>0.05$).

FIGURE S11. Number of myelinated anterior cingulate cortex fibers analysed by CARS based on their axonal diameter

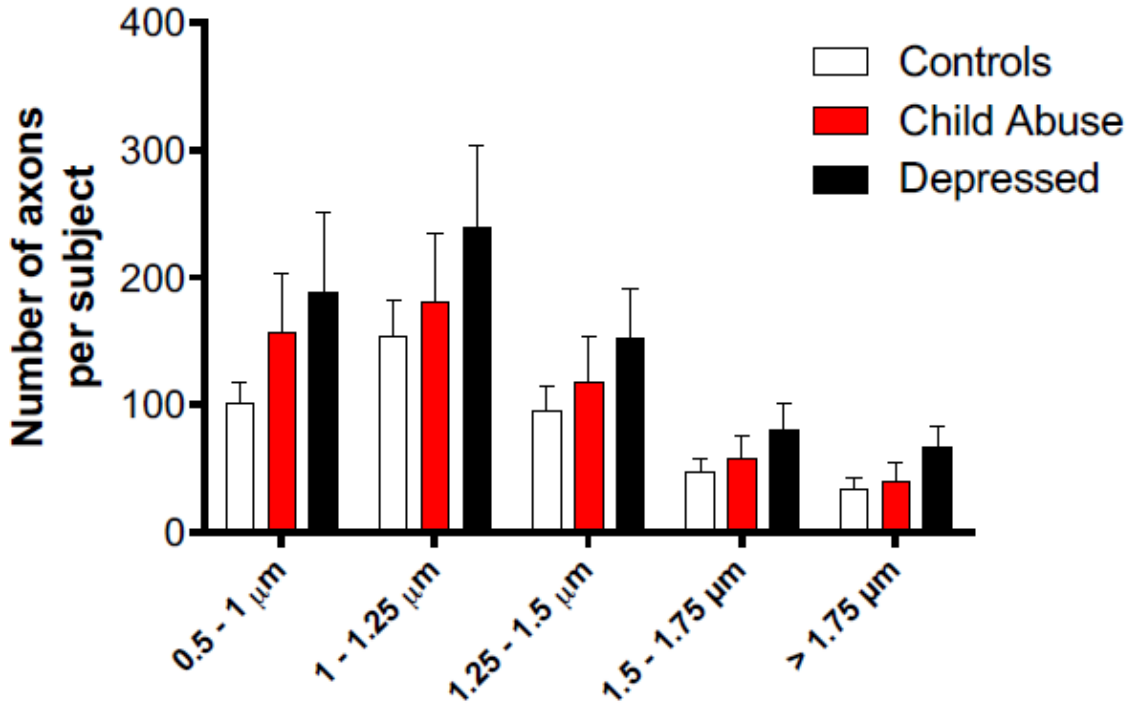

Comparable numbers of fibers were analysed in Controls (N=13), Child Abuse (N=11) and Depressed (N=10) subjects. Fibers of intermediate (1 to 1.25 µm) calibers are however enriched in the anterior cingulate cortex compared to smaller (0.5 to 1 µm) and larger (> 1.25 µm) axons (Two-way repeated measures ANOVA with diameter class as within factor and group as between factor; group effect: $F(2, 31) = 1.023$, $P > 0.05$; diameter class effect: $F(4, 124) = 31.76$, $P < 0.0001$; class x group interaction: $F(8, 124) = 0.6499$, $P > 0.05$). Data represent mean ± sem.

FIGURE S12. Scatter plots and linear fits of the axon diameter versus myelin thickness of individual fibers detected by CARS

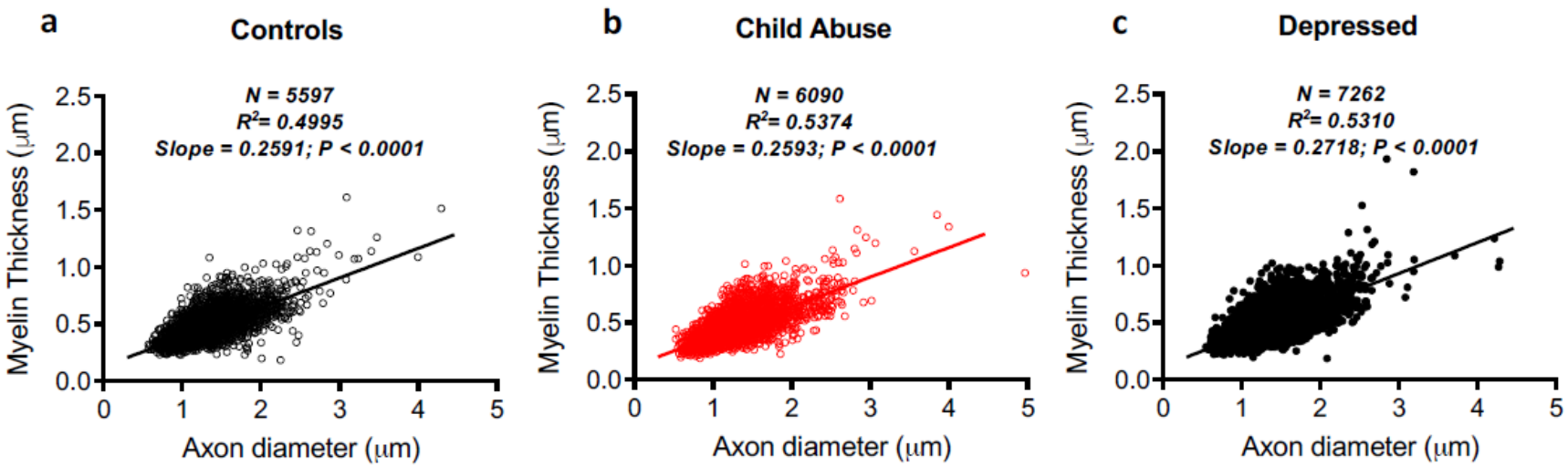

Scatter plots and linear fits of the axon diameter versus myelin thickness of individual fibers detected by CARS in the anterior cingulate cortex of Controls (left, N = 5597), Child Abuse (middle, N= 6090) and Depressed (right, N= 7262). A highly significant regression was found for the three groups, owing to the previously described increase in myelination of larger caliber fibers (Controls: R^2= 0.4995, Slope = 0.2591; P < 0.0001; Child Abuse: R^2= 0.5374, Slope = 0.2593; P < 0.0001; Depressed: R^2= 0.5310, Slope = 0.2718; P < 0.0001).

FIGURE S13. Effects of age and postmortem interval (PMI) on the morphometric measures analysed by CARS in the anterior cingulate cortex

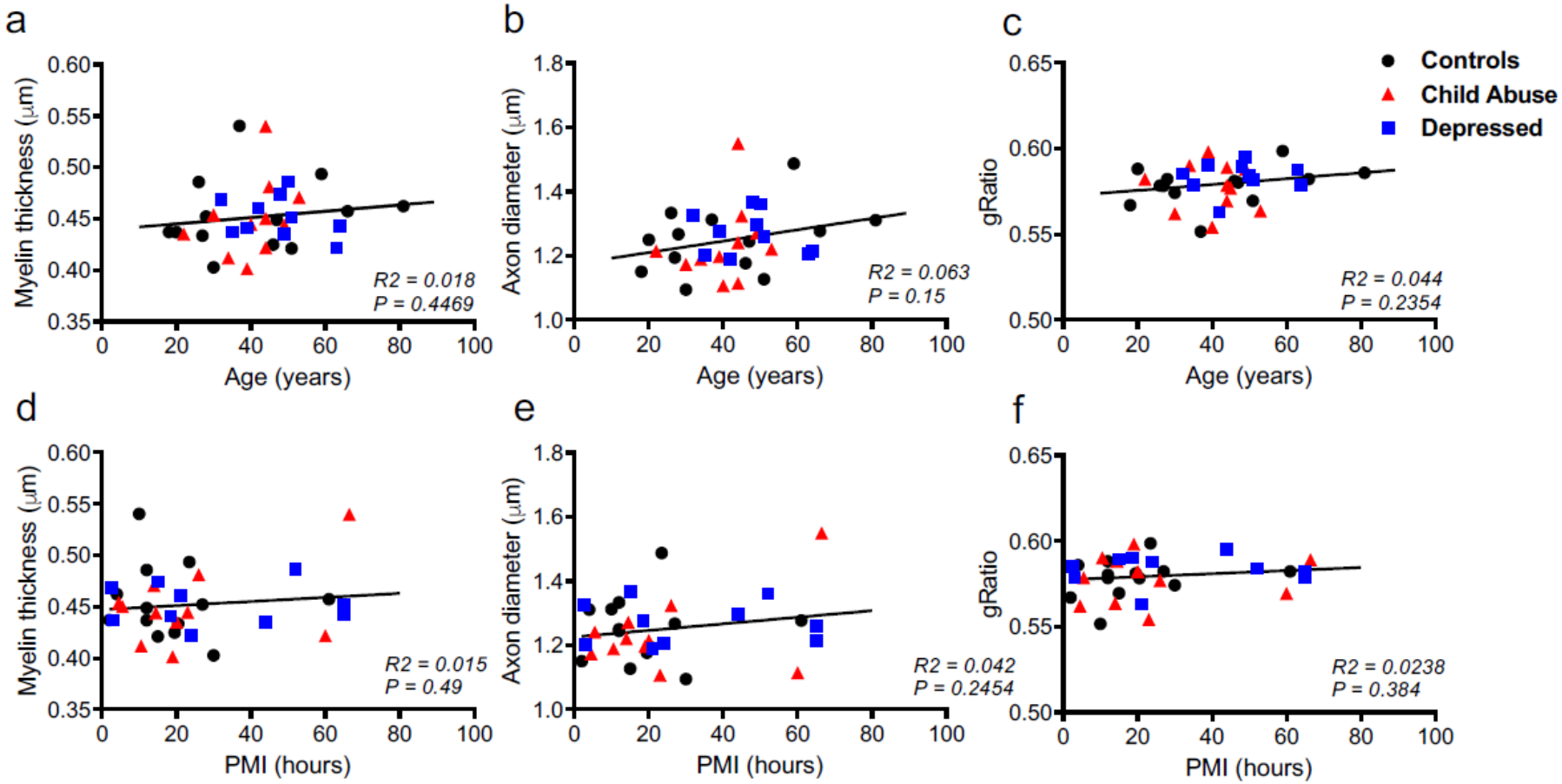

No relationship was found to be significant between age (**a-c**) or PMI (**d-f**) and myelin thickness, axon diameter and g-ratio. Each dot corresponds to the mean of all fibers from a subject for a given morphometric variable.

TABLE S1. Cohort demographics and covariates

group	Race	Gender	Age (years)	PMI (hours)	pH	RIN	Cause of death
Control	Caucasian	Male	19	32	6.55	6.5	Car accident polytrauma
Control	Caucasian	Male	47	12	6.49	8.7	Myocardial ischemia
Control	Caucasian	Male	30	30	6.37	7.5	Respiratory failure
Control	Caucasian	Male	28	27	6.32	6.9	Car accident polytrauma
Control	Caucasian	Male	41	24	6	7.5	Miocardial infraction
Control	Caucasian	Male	31	29.5	6.67	7.2	Car accident polytrauma
Control	Caucasian	Male	46	19.5	6.42	6.7	Myocardial infarction
Control	Caucasian	Male	27	20.5	6.55	7.7	lymphocytic myocarditis
Control	Caucasian	Male	51	15	6.83	6.9	Car accident
Control	Caucasian	Male	15	27	6.72	6.9	Accidental Hanging
Control	Caucasian	Male	42	63	6.75	6.9	Car accident polytrauma
Control	Caucasian	Male	18	2	6.87	6.5	Hypertrophic cardiomyopathy
Control	Caucasian	Female	66	61	6.8	6.9	Car accident polytrauma
Control	Caucasian	Male	37	10	6.7	6.8	Cardiorespiratory arrest
Control	Caucasian	Female	79	7.5	6.4	6.9	Malignant cardiac arrhythmia
Control	Caucasian	Male	20	12	6.3	6.7	Car accident
Control	Caucasian	Female	72	17	6.1	5.9	Myocardial infarction
Control	Caucasian	Male	81	4	5.8	5.7	Hemorrhage
Control	Caucasian	Male	55	21	6.7	6.4	Acute myocardial insufficiency
Control	Caucasian	Female	76	7	6.5	6.4	Hemorrhage
Control	Caucasian	Female	51	20	6.5	6.5	Pulmonary embolism
Control	Caucasian	Male	61	76.5	6.37	6.5	Cranial trauma
Control	Caucasian	Male	59	23.5	6.76	7	Car accident polytrauma
Control	Caucasian	Female	81	3	5.91	7.1	Respiratory failure
Control	Caucasian	Male	26	12	6.75	6.5	Car accident polytrauma
Control	Caucasian	Male	44	66	6.2	-	Respiratory failure
Mean			46.3	24.7	6.5	6.8	
S.E.M			4.1	4.0	0.1	0.1	
group	**Race**	**Gender**	**Age (years)**	**PMI (hours)**	**pH**	**RIN**	**Cause of death**
Child Abuse	Caucasian	Male	40	23	6.21	6.3	Hanging
Child Abuse	Caucasian	Male	26	21.5	5.5	-	Drugs with Sedative Effects
Child Abuse	Caucasian	Male	19	29.5	6.17	7.4	Hanging
Child Abuse	Caucasian	Male	45	20.5	6.57	7.5	Gunshot wound
Child Abuse	Caucasian	Male	53	14	6.64	9.1	Drugs with Sedative Effects
Child Abuse	Caucasian	Male	39	25.5	6.6	7.1	Hanging

Child Abuse	Caucasian	Male	22	11.5	6.35	8.7	Hanging
Child Abuse	Caucasian	Male	45	26	6.3	6.4	Drugs with Sedative Effects
Child Abuse	Caucasian	Male	26	34	6.67	7	Hanging
Child Abuse	Caucasian	Male	53	33.5	6.91	6.4	Hanging
Child Abuse	Caucasian	Male	39	19	6	6.1	Drugs without Sedative Effects
Child Abuse	Caucasian	Male	22	20	6.71	6.5	Hanging
Child Abuse	Caucasian	Female	65	64	6.31	5.7	Jumping
Child Abuse	Caucasian	Male	51	54	6.74	7.4	Drugs with Sedative Effects
Child Abuse	Caucasian	Female	54	28.5	6.77	6.9	Drugs with Sedative Effects
Child Abuse	Caucasian	Female	44	60	6.86	6.6	Jumping
Child Abuse	Caucasian	Male	42	19	6.78	6.9	Drugs with Sedative Effects
Child Abuse	Caucasian	Female	49	14.5	7.5	6.8	Drugs with Sedative Effects
Child Abuse	Caucasian	Female	55	2.5	6.5	7	Hanging
Child Abuse	Caucasian	Male	39	4	6.7	6.2	Hanging
Child Abuse	Caucasian	Male	30	4.5	6.7	6.8	Hanging
Child Abuse	Caucasian	Male	34	10.5	7	6.8	Hanging
Child Abuse	Caucasian	Male	34	4.5	6.45	7	Hanging
Child Abuse	Caucasian	Female	85	5	6.5	5.5	Drugs with Sedative Effects
Child Abuse	Caucasian	Male	44	66.5	7	6.8	Hanging
Child Abuse	Caucasian	Male	44	5.5	6.4	6.5	Drugs with Sedative Effects
Child Abuse	Caucasian	Female	25	56	6.55	6.1	Hanging
Mean			41.6	25.1	6.6	6.8	
S.E.M			2.8	3.7	0.1	0.2	
group	**Race**	**Gender**	**Age (years)**	**PMI (hours)**	**pH**	**RIN**	**Cause of death**
Depressed	Caucasian	Male	53	29	6.3	-	Hanging
Depressed	Caucasian	Male	42	21	6.4	6.8	Drowning
Depressed	Caucasian	Male	49	32	6.57	-	Hanging
Depressed	Caucasian	Male	18	27	6.22	-	Drugs with Sedative Effects
Depressed	Caucasian	Male	48	15	6.78	6.2	Jumping
Depressed	Caucasian	Female	55	36	6.79	-	Hanging

Depressed	Caucasian	Male	53	41	6.89	-	Hanging
Depressed	Caucasian	Male	39	18.5	6.37	6.6	Drowning
Depressed	Caucasian	Male	51	65	7.01	6.2	Hanging
Depressed	Caucasian	Male	48	49	6.56	-	Hanging
Depressed	Caucasian	Female	51	36	6.86	-	Hanging
Depressed	Caucasian	Male	50	52	6.81	6.6	Hanging
Depressed	Caucasian	Male	49	44	6.92	6.5	Hanging
Depressed	Caucasian	Male	47	2.5	6.79	-	Drugs with Sedative Effects
Depressed	Caucasian	Male	63	24	6.6	6.8	Hanging
Depressed	Caucasian	Male	77	4	6.3	7.3	Hanging
Depressed	Caucasian	Male	49	2.5	6.7	6.1	Hanging
Depressed	Caucasian	Male	64	6.5	6.25	6.4	Hanging
Depressed	Caucasian	Male	38	4	6.5	-	Drugs with Sedative Effects
Depressed	Caucasian	Male	35	3	6.5	6.7	Hanging
Depressed	Caucasian	Male	52	9.5	6.2	6.2	Hanging
Depressed	Caucasian	Male	60	65	6.2	-	Hanging
Depressed	Caucasian	Female	36	7.5	6.9	-	Hanging
Depressed	Caucasian	Male	32	2.5	6.11	6.6	Hanging
Depressed	Caucasian	Male	45	3	7.45	6.1	Drugs without Sedative Effects
Mean			48.2	24.0	6.6	6.5	
S.E.M			2.3	20.2	0.1	0.1	

TABLE S2. RRBS quality controls

	Controls (N=25 libraries)	**Child Abuse** (N=27 libraries)
Total reads	21.4E+6	21.7E+6
Aligned reads	9.2E+6	9.4E+6
Bisulfite conversion efficiency	99.2	99.2
Number of CpGs covered at 1X	1.11E+6	1.10E+6
Number of CpGs covered at 5X	6.96E+5	6.95E+5
Number of CpGs covered at 10X	5.51E+5	5.59E+5

TABLE S3. Primers used for amplification of genomic DNA in Targeted Bisulfite-Sequencing

Gene	**Targeted DNA strand**	**Primer**	**Primer Sequence**	**Primer length (bp)**
LINGO3	minus	Forward	TAY GTT GGA GGA GAG TAT TTT T	22
		Reverse	TCA CCC AAA CCA CRA TAA	18
POU3F1	minus	Forward	YGA AGT GTA GAA GTT GAT GTA TTA	24
		Reverse	ATA CTA CCC TAC RCC CAT ACC	21
ITGB1	minus	Forward	TTT TTT YGA YGA GTA AAG GGT T	22
		Reverse	CAA TTA CAT CTT CCA AAA ACR ATT T	25
MBP	minus	Forward	GAG GTT GAG AAT TTA GAG AAA GAT TTT	27
		Reverse	CAA ATC CTC CCA AAA CAC TC	20
CNTNAP1	plus	Forward	AGG ATT AGG AAT TAG AGA GAG AGA GA	26
		Reverse	ACT CTA AAC TCC TAA ACC CAA CC	23

TABLE S4. Primers used for the second round of PCR amplification during Targeted BS-Seq. UniversalF and universalR sequences are shown in red and blue, respectively.

Gene	Targeted DNA strand	Primer	Primer Sequence	Primer length (bp)
LINGO3	minus	Forward	ACA CTG ACG ACA TGG TTC TAC ANN NTA YGT TGG AGG AGA GTA TTT TT	47
		Reverse	TAC GGT AGC AGA GAC TTG GTC TNN NTC ACC CAA ACC ACR ATA A	43
POU3F1	minus	Forward	ACA CTG ACG ACA TGG TTC TAC ANN NYG AAG TGT AGA AGT TGA TGT ATT A	49
		Reverse	TAC GGT AGC AGA GAC TTG GTC TNN NAT ACT ACC CTA CRC CCA TAC C	46
ITGB1	minus	Forward	ACA CTG ACG ACA TGG TTC TAC ANN NTT TTT TYG AYG AGT AAA GGG TT	47
		Reverse	TAC GGT AGC AGA GAC TTG GTC TNN NCA ATT ACA TCT TCC AAA AAC RAT TT	50
MBP	minus	Forward	ACA CTG ACG ACA TGG TTC TAC ANN NGA GGT TGA GAA TTT AGA GAA AGA TTT T	52
		Reverse	TAC GGT AGC AGA GAC TTG GTC TNN NCA AAT CCT CCC AAA ACA CTC	45
CNTNAP1	plus	Forward	ACA CTG ACG ACA TGG TTC TAC ANN NAG GAT TAG GAA TTA GAG AGA GAG AGA	51
		Reverse	TAC GGT AGC AGA GAC TTG GTC TNN NAC TCT AAA CTC CTA AAC CCA ACC	48

TABLE S5. Primers used for the third round of PCR amplification in NeuN+ nuclear fractions, during Targeted Bisulfite-Sequencing (Fig.1). Notes: (i) The same "P5-UniversalF" primer was use across all samples; (ii) Distinct "P7-UniversalR" primers, with different index sequences, were used for each sample (single-indexing strategy); (iii) UniversalF and UniversalR sequences are the same as those used during Round2 PCR amplification (see Table2); (iv) P5 and P7 sequences are indicated in red and blue, respectively, while 10-base index sequences are underlined; (v) Additional primers with distinct indices (not shown) were used during PCR amplification and indexing of Sox10+ fractions.

Primer+B8:E74	Sample#	Primer Sequence	Primer length (bp)
P5-UniversalF	1 to 77	AAT GAT ACG GCG ACC ACC GAG ATC T ACA CTG ACG ACA TGG TTC TAC A	47

Primer	Sample#	Primer Sequence	Primer length (bp)
P7-UniversalR	1	CAA GCA GAA GAC GGC ATA CGA GAT GTA TCG TCG T TAC GGT AGC AGA GAC TTG GTC T	56
P7-UniversalR	2	CAA GCA GAA GAC GGC ATA CGA GAT GTG TAT GCG T TAC GGT AGC AGA GAC TTG GTC T	56
P7-UniversalR	3	CAA GCA GAA GAC GGC ATA CGA GAT TGC TCG TAG T TAC GGT AGC AGA GAC TTG GTC T	56
P7-UniversalR	4	CAA GCA GAA GAC GGC ATA CGA GAT GTC GTC GTC T TAC GGT AGC AGA GAC TTG GTC T	56
P7-UniversalR	5	CAA GCA GAA GAC GGC ATA CGA GAT GTG CGT GTG T TAC GGT AGC AGA GAC TTG GTC T	56
P7-UniversalR	6	CAA GCA GAA GAC GGC ATA CGA GAT GCG TCG TGT A TAC GGT AGC AGA GAC TTG GTC T	56
P7-UniversalR	7	CAA GCA GAA GAC GGC ATA CGA GAT GTC GTG TAC T TAC GGT AGC AGA GAC TTG GTC T	56
P7-UniversalR	8	CAA GCA GAA GAC GGC ATA CGA GAT GAT GTA GCG T TAC GGT AGC AGA GAC TTG GTC T	56
P7-UniversalR	9	CAA GCA GAA GAC GGC ATA CGA GAT GAG TGA TCG T TAC GGT AGC AGA GAC TTG GTC T	56
P7-UniversalR	10	CAA GCA GAA GAC GGC ATA CGA GAT CGC TAT CAG T TAC GGT AGC AGA GAC TTG GTC T	56
P7-UniversalR	11	CAA GCA GAA GAC GGC ATA CGA GAT CGC TGT AGT C TAC GGT AGC AGA GAC TTG GTC T	56
P7-UniversalR	12	CAA GCA GAA GAC GGC ATA CGA GAT GCT AGT GAG T TAC GGT AGC AGA GAC TTG GTC T	56
P7-UniversalR	13	CAA GCA GAA GAC GGC ATA CGA GAT GAG CTA GTG A TAC GGT AGC AGA GAC TTG GTC T	56
P7-UniversalR	14	CAA GCA GAA GAC GGC ATA CGA GAT CGT GCT GTC A TAC GGT AGC AGA GAC TTG GTC T	56
P7-UniversalR	15	CAA GCA GAA GAC GGC ATA CGA GAT GAT CGT CTC T TAC GGT AGC AGA GAC TTG GTC T	56
P7-UniversalR	16	CAA GCA GAA GAC GGC ATA CGA GAT GTG CTG TCG T TAC GGT AGC AGA GAC TTG GTC T	56

P7-UniversalR	17	CAA GCA GAA GAC GGC ATA CGA GAT TGA GCG TGC T TAC GGT AGC AGA GAC TTG GTC T	56
P7-UniversalR	18	CAA GCA GAA GAC GGC ATA CGA GAT CAT GTC GTC A TAC GGT AGC AGA GAC TTG GTC T	56
P7-UniversalR	19	CAA GCA GAA GAC GGC ATA CGA GAT TCA GTG TCT C TAC GGT AGC AGA GAC TTG GTC T	56
P7-UniversalR	20	CAA GCA GAA GAC GGC ATA CGA GAT GTG CTC ATG T TAC GGT AGC AGA GAC TTG GTC T	56
P7-UniversalR	21	CAA GCA GAA GAC GGC ATA CGA GAT CGT ATC TCG A TAC GGT AGC AGA GAC TTG GTC T	56
P7-UniversalR	22	CAA GCA GAA GAC GGC ATA CGA GAT GTC ATG CGT C TAC GGT AGC AGA GAC TTG GTC T	56
P7-UniversalR	23	CAA GCA GAA GAC GGC ATA CGA GAT CTA TGC GAT C TAC GGT AGC AGA GAC TTG GTC T	56
P7-UniversalR	24	CAA GCA GAA GAC GGC ATA CGA GAT TGC TAT GCT G TAC GGT AGC AGA GAC TTG GTC T	56
P7-UniversalR	25	CAA GCA GAA GAC GGC ATA CGA GAT TGT GTG CAT G TAC GGT AGC AGA GAC TTG GTC T	56
P7-UniversalR	26	CAA GCA GAA GAC GGC ATA CGA GAT GAG TGT CAC T TAC GGT AGC AGA GAC TTG GTC T	56
P7-UniversalR	27	CAA GCA GAA GAC GGC ATA CGA GAT CTA GTC TCG T TAC GGT AGC AGA GAC TTG GTC T	56
P7-UniversalR	28	CAA GCA GAA GAC GGC ATA CGA GAT GAG TGC ATC T TAC GGT AGC AGA GAC TTG GTC T	56
P7-UniversalR	29	CAA GCA GAA GAC GGC ATA CGA GAT TGC GTA GTC G TAC GGT AGC AGA GAC TTG GTC T	56
P7-UniversalR	30	CAA GCA GAA GAC GGC ATA CGA GAT CTG TGT CGT C TAC GGT AGC AGA GAC TTG GTC T	56
P7-UniversalR	31	CAA GCA GAA GAC GGC ATA CGA GAT CTG TAG TGC G TAC GGT AGC AGA GAC TTG GTC T	56
P7-UniversalR	32	CAA GCA GAA GAC GGC ATA CGA GAT GTG CGC TAG T TAC GGT AGC AGA GAC TTG GTC T	56
P7-UniversalR	33	CAA GCA GAA GAC GGC ATA CGA GAT TGT GCT CGC A TAC GGT AGC AGA GAC TTG GTC T	56
P7-UniversalR	34	CAA GCA GAA GAC GGC ATA CGA GAT GAT GCG AGC T TAC GGT AGC AGA GAC TTG GTC T	56
P7-UniversalR	35	CAA GCA GAA GAC GGC ATA CGA GAT CTG TAC GTG A TAC GGT AGC AGA GAC TTG GTC T	56
P7-UniversalR	36	CAA GCA GAA GAC GGC ATA CGA GAT GCG ATG ATG A TAC GGT AGC AGA GAC TTG GTC T	56
P7-UniversalR	37	CAA GCA GAA GAC GGC ATA CGA GAT TGT CGA GTC A TAC GGT AGC AGA GAC TTG GTC T	56
P7-UniversalR	38	CAA GCA GAA GAC GGC ATA CGA GAT GTC TAC TGT C TAC GGT AGC AGA GAC TTG GTC T	56
P7-UniversalR	39	CAA GCA GAA GAC GGC ATA CGA GAT CAG TCA GAG T TAC GGT AGC AGA GAC TTG GTC T	56
P7-UniversalR	40	CAA GCA GAA GAC GGC ATA CGA GAT CGC AGT CTA T TAC GGT AGC AGA GAC TTG GTC T	56
P7-UniversalR	41	CAA GCA GAA GAC GGC ATA CGA GAT GTA TGA GCA C TAC GGT AGC AGA GAC TTG GTC T	56
P7-UniversalR	42	CAA GCA GAA GAC GGC ATA CGA GAT CGA GTG CTG T TAC GGT AGC AGA GAC TTG GTC T	56
P7-UniversalR	43	CAA GCA GAA GAC GGC ATA CGA GAT TAT AGC ACG C TAC GGT AGC AGA GAC TTG GTC T	56
P7-UniversalR	44	CAA GCA GAA GAC GGC ATA CGA GAT TCA TGC GCG A TAC GGT AGC AGA GAC TTG GTC T	56

P7-UniversalR	45	CAA GCA GAA GAC GGC ATA CGA GAT TAT GCG CTG C TAC GGT AGC AGA GAC TTG GTC T	56
P7-UniversalR	46	CAA GCA GAA GAC GGC ATA CGA GAT TCT CTG TGC A TAC GGT AGC AGA GAC TTG GTC T	56
P7-UniversalR	47	CAA GCA GAA GAC GGC ATA CGA GAT CTA TCG CGT G TAC GGT AGC AGA GAC TTG GTC T	56
P7-UniversalR	48	CAA GCA GAA GAC GGC ATA CGA GAT TAC GCT GCT G TAC GGT AGC AGA GAC TTG GTC T	56
P7-UniversalR	49	CAA GCA GAA GAC GGC ATA CGA GAT CTG CAT GAT C TAC GGT AGC AGA GAC TTG GTC T	56
P7-UniversalR	50	CAA GCA GAA GAC GGC ATA CGA GAT CGC GTA TCA T TAC GGT AGC AGA GAC TTG GTC T	56
P7-UniversalR	51	CAA GCA GAA GAC GGC ATA CGA GAT GTA TCT CTC G TAC GGT AGC AGA GAC TTG GTC T	56
P7-UniversalR	52	CAA GCA GAA GAC GGC ATA CGA GAT GCT CAT ATG C TAC GGT AGC AGA GAC TTG GTC T	56
P7-UniversalR	53	CAA GCA GAA GAC GGC ATA CGA GAT CAC TAT GTC G TAC GGT AGC AGA GAC TTG GTC T	56
P7-UniversalR	54	CAA GCA GAA GAC GGC ATA CGA GAT TAG CGC GTA G TAC GGT AGC AGA GAC TTG GTC T	56
P7-UniversalR	55	CAA GCA GAA GAC GGC ATA CGA GAT CGT CAC AGT A TAC GGT AGC AGA GAC TTG GTC T	56
P7-UniversalR	56	CAA GCA GAA GAC GGC ATA CGA GAT TCG CGT GAG A TAC GGT AGC AGA GAC TTG GTC T	56
P7-UniversalR	57	CAA GCA GAA GAC GGC ATA CGA GAT TAC ATC GCT G TAC GGT AGC AGA GAC TTG GTC T	56
P7-UniversalR	58	CAA GCA GAA GAC GGC ATA CGA GAT GTG AGA GAC A TAC GGT AGC AGA GAC TTG GTC T	56
P7-UniversalR	59	CAA GCA GAA GAC GGC ATA CGA GAT GAC TGT ACG T TAC GGT AGC AGA GAC TTG GTC T	56
P7-UniversalR	60	CAA GCA GAA GAC GGC ATA CGA GAT GCA CGT AGC T TAC GGT AGC AGA GAC TTG GTC T	56
P7-UniversalR	61	CAA GCA GAA GAC GGC ATA CGA GAT TCA CGC TAT G TAC GGT AGC AGA GAC TTG GTC T	56
P7-UniversalR	62	CAA GCA GAA GAC GGC ATA CGA GAT CGT ACT ACG T TAC GGT AGC AGA GAC TTG GTC T	56
P7-UniversalR	63	CAA GCA GAA GAC GGC ATA CGA GAT CAG CTG AGT A TAC GGT AGC AGA GAC TTG GTC T	56
P7-UniversalR	64	CAA GCA GAA GAC GGC ATA CGA GAT GAG ATC AGT C TAC GGT AGC AGA GAC TTG GTC T	56
P7-UniversalR	65	CAA GCA GAA GAC GGC ATA CGA GAT TAC TGA GCT G TAC GGT AGC AGA GAC TTG GTC T	56
P7-UniversalR	66	CAA GCA GAA GAC GGC ATA CGA GAT TAG TAG CGC G TAC GGT AGC AGA GAC TTG GTC T	56
P7-UniversalR	67	CAA GCA GAA GAC GGC ATA CGA GAT GAC GTC TGC T TAC GGT AGC AGA GAC TTG GTC T	56
P7-UniversalR	68	CAA GCA GAA GAC GGC ATA CGA GAT GTA CTC GCG A TAC GGT AGC AGA GAC TTG GTC T	56
P7-UniversalR	69	CAA GCA GAA GAC GGC ATA CGA GAT TCT GAG CGC A TAC GGT AGC AGA GAC TTG GTC T	56
P7-UniversalR	70	CAA GCA GAA GAC GGC ATA CGA GAT TAG ACG TGC T TAC GGT AGC AGA GAC TTG GTC T	56
P7-UniversalR	71	CAA GCA GAA GAC GGC ATA CGA GAT GTG ACT CGT C TAC GGT AGC AGA GAC TTG GTC T	56
P7-UniversalR	72	CAA GCA GAA GAC GGC ATA CGA GAT TCG AGT AGC G TAC GGT AGC AGA GAC TTG GTC T	56

P7-UniversalR	73	CAA GCA GAA GAC GGC ATA CGA GAT CGT ATG ATG T TAC GGT AGC AGA GAC TTG GTC T	56
P7-UniversalR	74	CAA GCA GAA GAC GGC ATA CGA GAT TAG TCT GTC A TAC GGT AGC AGA GAC TTG GTC T	56
P7-UniversalR	75	CAA GCA GAA GAC GGC ATA CGA GAT TGT CTC TAT C TAC GGT AGC AGA GAC TTG GTC T	56

TABLE S6. RNA-Sequencing quality controls

	Controls (N=24 libraries)	**Child Abuse** (N=26 libraries)	**t-test (p-value)**
RIN	6.6 ± 0.25	6.8 ± 0.15	0.34
Number of reads (million)	61.7 ± 1.6	62.2 ± 2.7	0.87
Average phred score	34.4 ± 0.14	34.5 ± 0.11	0.52
Duplicates (%)	30.6 ± 2.5	29.5 ± 1.7	0.62

TABLE S7. Primers used for Reverse transcription-PCR

Gene	**Primer**	**Primer Sequence**	**Primer length (bp)**	**Amplicon size (bp)**
ITGB1	Forward	GCC GCG CGG AAA AGA TGA AT	20	166
	Reverse	GAA TTT GTG CAC CAC CCA CAA	21	
GAPDH	Forward	TTG TCA AGC TCA TTT CCT GG	20	202
	Reverse	TGT GAG GAG GGG AGA TTC AG	20	
b-Actin	Forward	AAG ACC TGT ACG CCA ACA CA	20	85
	Reverse	GCA GTG ATC TCC TTC TGC ATC	21	

TABLE S8. Summary of main genes identified as differentially methylated (RRBS) or differentially expressed (RNASequencing) in the present study, and that were further validated using fluorescence-activated cell sorting and Targeted BSSequencing (RRBS validation), or Nanostring and qPCR (RNA-Seq validation).

Gene ID	Official Full Name	Technique	Observed change in child abused subjects	Tissue or cell-type affected
LINGO3	Leucine rich repeat and Ig domain containing 3	RRBS	Decreased DNA methylation	Whole tissue
		FACS & Targeted BS-Seq (RRBS validation)		Oligodendrocytes
POU3F1	POU domain, class 3, transcription factor 1	RRBS	Decreased DNA methylation	Whole tissue
		FACS & Targeted BS-Seq (RRBS validation)		Oligodendrocytes
ITGB1	Integrin subunit beta 1	RRBS	Increased DNA methylation	Whole tissue
KLK6	Kallikrein related peptidase	RNA-Sequencing	Decreased expression	Whole tissue
		Nanostring (RNA-Sequencing validation)		
MOBP	Myelin-associated oligodendrocyte basic protein	RNA-Sequencing		
		Nanostring (RNA-Sequencing validation)		
PLP1	Proteolipid protein 1	RNA-Sequencing		
		Nanostring (RNA-Sequencing validation)		
MBP	Myelin basic protein	RNA-Sequencing		
		Nanostring (RNA-Sequencing validation)		
MAG	Myelin-associated glycoprotein	RNA-Sequencing		
		Nanostring (RNA-Sequencing validation)		
PLLP	Plasmolipin	RNA-Sequencing		
		Nanostring (RNA-Sequencing validation)		
CD9	CD9 molecule	RNA-Sequencing		
		Nanostring (RNA-Sequencing validation)		
MOG	Myelin oligodendrocyte glycoprotein	RNA-Sequencing		
		Nanostring (RNA-Sequencing validation)		
ITGB1	Integrin subunit beta 1	RNA-Sequencing		
		qPCR (RNA-Sequencing validation)		
CNTNAP1	Contacting associated protein-like 1	RNA-Sequencing		
		Nanostring (RNA-Sequencing validation)		

TABLE S9. Summary of the 20 gene lists showing the highest enrichment scores in the Gene Set Enrichment Analysis (GSEA). This analysis was conducted on RNA-Sequencing data as described in supplementary material and methods.

N	List Name	Enrichment score (ES)	Enrichment in UP or DOWN regulated genes	Number of genes in list
1	LEIN_OLIGODENDROCYTE_MARKERS	-0.753	Down	72
2	BROWNE_INTERFERON_RESPONSIVE_GENES	-0.736	Down	59
3	SANA_RESPONSE_TO_IFNG_UP	-0.712	Down	65
4	HECKER_IFNB1_TARGETS	-0.703	Down	74
5	WIELAND_UP_BY_HBV_INFECTION	-0.699	Down	84
6	LEIN_NEURON_MARKERS	0.687	Up	66
7	LU_AGING_BRAIN_UP	-0.674	Down	258
8	ASTON_MAJOR_DEPRESSIVE_DISORDER_DN	-0.669	Down	154
9	MCLACHLAN_DENTAL_CARIES_UP	-0.651	Down	200
10	MCLACHLAN_DENTAL_CARIES_DN	-0.626	Down	200
11	REACTOME_RESPIRATORY_ELECTRON_TRANSPORT	0.626	Up	63
12	REACTOME_RESPIRATORY_ELECTRON_TRANSPORT_ATP_SYNTHESIS_BY_CHEMIOSMOTIC_COUPLING_AND_HEAT_PRODUCTION_BY_UNCOUPLING_PROTEINS	0.602	Up	78
13	MOOTHA_VOXPHOS	0.581	Up	86
14	KEGG_CARDIAC_MUSCLE_CONTRACTION	0.578	Up	60
15	SCHUETZ_BREAST_CANCER_DUCTAL_INVASIVE_UP	-0.565	Down	321
16	KEGG_OXIDATIVE_PHOSPHORYLATION	0.542	Up	104
17	NIKOLSKY_BREAST_CANCER_16P13_AMPLICON	0.522	Up	88
18	KEGG_PARKINSONS_DISEASE	0.513	Up	103
19	MIKKELSEN_MCV6_HCP_WITH_H3K27ME3	0.449	Up	324
20	MIKKELSEN_MEF_HCP_WITH_H3K27ME3	0.422	Up	405

TABLE S10. Demographics of postmortem human brain samples used for Coherent anti-Stokes Raman Scattering microscopy

Group	Race	Gender	Age (years)	PMI (hours)	pH	RIN
Control	Caucasian	Male	47	12	6.49	8.7
Control	Caucasian	Male	30	30	6.37	7.5
Control	Caucasian	Male	28	27	6.32	6.9
Control	Caucasian	Male	46	19.5	6.42	6.7
Control	Caucasian	Male	27	20.5	6.55	7.7
Control	Caucasian	Male	51	15	6.83	6.9
Control	Caucasian	Male	18	2	6.87	6.5
Control	Caucasian	Female	66	61	6.8	6.9
Control	Caucasian	Male	37	10	6.7	6.8
Control	Caucasian	Male	20	12	6.3	6.7
Control	Caucasian	Male	81	4	5.8	5.7
Control	Caucasian	Male	59	23.5	6.76	7
Control	Caucasian	Male	26	12	6.75	6.5
		Mean	41.23076923	19.11538462	6.535385	6.961538
		S.E.M	5.31465541	4.18297597	0.083125	0.196944
Group	**Race**	**Gender**	**Age (years)**	**PMI (hours)**	**pH**	**RIN**
Child Abuse	Caucasian	Male	40	23	6.21	6.3
Child Abuse	Caucasian	Male	53	14	6.64	9.1
Child Abuse	Caucasian	Male	45	26	6.3	6.4
Child Abuse	Caucasian	Male	39	19	6	6.1
Child Abuse	Caucasian	Male	22	20	6.71	6.5
Child Abuse	Caucasian	Female	44	60	6.86	6.6
Child Abuse	Caucasian	Female	49	14.5	7.5	6.8
Child Abuse	Caucasian	Male	30	4.5	6.7	6.8
Child Abuse	Caucasian	Male	34	10.5	7	6.8
Child Abuse	Caucasian	Male	44	66.5	7	6.8
Child Abuse	Caucasian	Male	44	5.5	6.4	6.5
		Mean	40.36363636	23.95454545	6.665455	6.790909
		S.E.M	2.667217574	6.210860922	0.128497	0.24138
Group	**Race**	**Gender**	**Age (years)**	**PMI (hours)**	**pH**	**RIN**
Depressed	Caucasian	Male	42	21	6.4	6.8
Depressed	Caucasian	Male	48	15	6.78	6.2
Depressed	Caucasian	Male	39	18.5	6.37	6.6
Depressed	Caucasian	Male	51	65	7.01	6.2
Depressed	Caucasian	Male	50	52	6.81	6.6
Depressed	Caucasian	Male	49	44	6.92	6.5
Depressed	Caucasian	Male	63	24	6.6	6.8
Depressed	Caucasian	Male	64	6.5	6.25	6.4

Depressed	Caucasian	Male	35	3	6.5	6.7
Depressed	Caucasian	Male	32	2.5	6.11	6.6
		Mean	47.3	25.15	6.575	6.54
		S.E.M	3.386410751	6.816259157	0.094648	0.068638

REFERENCES

1. Dumais A, Lesage AD, Alda M, Rouleau G, Dumont M, Chawky N, Roy M, Mann JJ, Benkelfat C, Turecki G. Risk factors for suicide completion in major depression: a case-control study of impulsive and aggressive behaviors in men. Am J Psychiatry. 2005;162:2116-2124.
2. Brewin CR, Andrews B, Gotlib IH. Psychopathology and early experience: a reappraisal of retrospective reports. Psychol Bull. 1993;113:82-98.
3. Conner KR, Conwell Y, Duberstein PR. The validity of proxy-based data in suicide research: a study of patients 50 years of age and older who attempted suicide. II. Life events, social support and suicidal behavior. Acta Psychiatr Scand. 2001;104:452-457.
4. Hawton K, Appleby L, Platt S, Foster T, Cooper J, Malmberg A, Simkin S. The psychological autopsy approach to studying suicide: a review of methodological issues. J Affect Disord. 1998;50:269-276.
5. Kelly TM, Mann JJ. Validity of DSM-III-R diagnosis by psychological autopsy: a comparison with clinician ante-mortem diagnosis. Acta Psychiatr Scand. 1996;94:337-343.
6. McGirr A, Tousignant M, Routhier D, Pouliot L, Chawky N, Margolese HC, Turecki G. Risk factors for completed suicide in schizophrenia and other chronic psychotic disorders: a case-control study. Schizophr Res. 2006;84:132-143.
7. Brent DA, Perper JA, Moritz G, Allman CJ, Roth C, Schweers J, Balach L. The validity of diagnoses obtained through the psychological autopsy procedure in adolescent suicide victims: use of family history. Acta Psychiatr Scand. 1993;87:118-122.
8. Bifulco A, Brown GW, Harris TO. Childhood Experience of Care and Abuse (CECA): a retrospective interview measure. J Child Psychol Psychiatry. 1994;35:1419-1435.
9. Bifulco A, Brown GW, Lillie A, Jarvis J. Memories of childhood neglect and abuse: corroboration in a series of sisters. J Child Psychol Psychiatry. 1997;38:365-374.
10. Mai JK, Paxinos G, Voss T. Atlas of the Human Brain, Third Edition. Elsevier Science. 2007.
11. Labonte B, Suderman M, Maussion G, Navaro L, Yerko V, Mahar I, Bureau A, Mechawar N, Szyf M, Meaney MJ, Turecki G. Genome-wide epigenetic regulation by early-life trauma. Arch Gen Psychiatry. 2012;69:722-731.
12. Chen GG, Diallo AB, Poujol R, Nagy C, Staffa A, Vaillancourt K, Lutz PE, Ota V, Mash DC, Turecki G, Ernst C. BisQC: an operational pipeline for multiplexed bisulfite sequencing. BMC Genomics. 2014;15:290.
13. Meissner A, Gnirke A, Bell GW, Ramsahoye B, Lander ES, Jaenisch R. Reduced representation bisulfite sequencing for comparative high-resolution DNA methylation analysis. Nucleic Acids Res. 2005;33:5868-5877.
14. Krueger F, Andrews SR. Bismark: a flexible aligner and methylation caller for Bisulfite-Seq applications. Bioinformatics. 2011;27:1571-1572.
15. Jaffe AE, Murakami P, Lee H, Leek JT, Fallin MD, Feinberg AP, Irizarry RA. Bump hunting to identify differentially methylated regions in epigenetic epidemiology studies. Int J Epidemiol. 2012;41:200-209.
16. Chen GG, Gross JA, Lutz PE, Vaillancourt K, Maussion G, Bramoulle A, Théroux JF, Bouret G, Masurel A, Lepage P, Turecki G, Ernst C. A medium throughput bisulfite sequencing approach to analyze 5-methylcytosine and 5-hydroxymethylcytosine In revision.

17. Chen ES, Gigek CO, Rosenfeld JA, Diallo AB, Maussion G, Chen GG, Vaillancourt K, Lopez JP, Crapper L, Poujol R, Shaffer LG, Bourque G, Ernst C. Molecular convergence of neurodevelopmental disorders. Am J Hum Genet. 2014;95:490-508.
18. Bolger AM, Lohse M, Usadel B. Trimmomatic: a flexible trimmer for Illumina sequence data. Bioinformatics. 2014;30:2114-2120.
19. Trapnell C, Pachter L, Salzberg SL. TopHat: discovering splice junctions with RNA-Seq. Bioinformatics. 2009;25:1105-1111.
20. Love MI, Huber W, Anders S. Moderated estimation of fold change and dispersion for RNA-seq data with DESeq2. Genome Biol. 2014;15:550.
21. Farmer WT, Abrahamsson T, Chierzi S, Lui C, Zaelzer C, Jones EV, Bally BP, Chen GG, Theroux JF, Peng J, Bourque CW, Charron F, Ernst C, Sjostrom PJ, Murai KK. Neurons diversify astrocytes in the adult brain through sonic hedgehog signaling. Science. 2016;351:849-854.
22. Maussion G, Diallo AB, Gigek CO, Chen ES, Crapper L, Theroux JF, Chen GG, Vasuta C, Ernst C. Investigation of genes important in neurodevelopment disorders in adult human brain. Hum Genet. 2015;134:1037-1053.
23. Anders S, Pyl PT, Huber W. HTSeq--a Python framework to work with high-throughput sequencing data. Bioinformatics. 2015;31:166-169.
24. Trabzuni D, Ramasamy A, Imran S, Walker R, Smith C, Weale ME, Hardy J, Ryten M, North American Brain Expression C. Widespread sex differences in gene expression and splicing in the adult human brain. Nat Commun. 2013;4:2771.
25. Erraji-Benchekroun L, Underwood MD, Arango V, Galfalvy H, Pavlidis P, Smyrniotopoulos P, Mann JJ, Sibille E. Molecular aging in human prefrontal cortex is selective and continuous throughout adult life. Biol Psychiatry. 2005;57:549-558.
26. Gallego Romero I, Pai AA, Tung J, Gilad Y. RNA-seq: impact of RNA degradation on transcript quantification. BMC Biol. 2014;12:42.
27. Subramanian A, Tamayo P, Mootha VK, Mukherjee S, Ebert BL, Gillette MA, Paulovich A, Pomeroy SL, Golub TR, Lander ES, Mesirov JP. Gene set enrichment analysis: a knowledge-based approach for interpreting genome-wide expression profiles. Proc Natl Acad Sci U S A. 2005;102:15545-15550.
28. Lutz PE, Zhou Y, Labbe A, Mechawar N, Turecki G. Decreased expression of nociceptin/orphanin FQ in the dorsal anterior cingulate cortex of suicides. Eur Neuropsychopharmacol. 2015.
29. Geiss GK, Bumgarner RE, Birditt B, Dahl T, Dowidar N, Dunaway DL, Fell HP, Ferree S, George RD, Grogan T, James JJ, Maysuria M, Mitton JD, Oliveri P, Osborn JL, Peng T, Ratcliffe AL, Webster PJ, Davidson EH, Hood L, Dimitrov K. Direct multiplexed measurement of gene expression with color-coded probe pairs. Nat Biotechnol. 2008;26:317-325.
30. M'Boutchou M-N, van Kempen L. Analysis of the Tumor Microenvironment Transcriptome Via NanoString mRNA and miRNA Expression Profiling. The Tumor Microenvironment: Methods and Protocols (Methods in Molecular Biology). 2016;Humana Press; 1st ed. .
31. Champagne FA, Francis DD, Mar A, Meaney MJ. Variations in maternal care in the rat as a mediating influence for the effects of environment on development. Physiol Behav. 2003;79:359-371.
32. Francis DD, Champagne FC, Meaney MJ. Variations in maternal behaviour are associated with differences in oxytocin receptor levels in the rat. J Neuroendocrinol. 2000;12:1145-1148.

33. Liu D, Diorio J, Tannenbaum B, Caldji C, Francis D, Freedman A, Sharma S, Pearson D, Plotsky PM, Meaney MJ. Maternal care, hippocampal glucocorticoid receptors, and hypothalamic-pituitary-adrenal responses to stress. Science. 1997;277:1659-1662.
34. Belanger E, Turcotte R, Daradich A, Sadetsky G, Gravel P, Bachand K, De Koninck Y, Cote DC. Maintaining polarization in polarimetric multiphoton microscopy. J Biophotonics. 2015;8:884-888.
35. Begin S, Dupont-Therrien O, Belanger E, Daradich A, Laffray S, De Koninck Y, Cote DC. Automated method for the segmentation and morphometry of nerve fibers in large-scale CARS images of spinal cord tissue. Biomed Opt Express. 2014;5:4145-4161.
36. Bioud FZ, Gasecka P, Ferrand P, Rigneault H, Duboisset J, Brasselet S. Structure of molecular packing probed by polarization-resolved nonlinear four-wave mixing and coherent anti-Stokes Raman-scattering microscopy. Phys Rev A. 2014;89.